A System for In Situ UV-Visible Illumination of Transmission Electron Microscope Samples

by

Benjamin Miller

A Thesis Presented in Partial Fulfillment
of the Requirements for the Degree
Master of Science

Approved July 2012 by the
Graduate Supervisory Committee:

Peter Crozier, Chair
Martha McCartney
Peter Rez

ARIZONA STATE UNIVERSITY
August 2012

ABSTRACT

A system for illuminating a sample *in situ* with visible and UV light inside a transmission electron microscope was devised to study photocatalysts. There are many factors which must be considered when designing and building such a system. These include both mechanical, optical, and electron optical considerations. Some of the restrictions posed by the electron microscope column are significant, and care must be taken not to degrade the microscope's electron optical performance, or to unduly restrict the other current capabilities of the microscope. The nature of these various design considerations is discussed in detail. A description of the system that has been added to the microscope at ASU, an FEI Tecnai F20 environmental transmission electron microscope is also given. The system includes a high brightness broadband light source with optical filters, a fiber to guide the light to the sample, and a system for precisely aligning the fiber tip. The spatial distribution and spectrum of the light reaching the sample has been characterized, and is described in detail.

ACKNOWLEDGEMENTS

This work could not have been possible without the guidance, assistance, insight, inspiration, and encouragement from my advisor, Dr. Peter Crozier. His contributions to this work and to the beginnings of my career have been invaluable.

I would also like to thank my committee members, Dr. Peter Rez, and Dr. Molly McCartney for their gracious agreement to serve on my committee and for their feedback.

I am also grateful to John Prince from ASU's Physics Machine Shop, for aiding in the design and overseeing the construction of the fiber manipulator, and to Karl Weiss, for invaluable suggestions and practical help in using the microscopy facilities at ASU.

I would also like to thank Zahra Hussaini who took measurements of the light's spatial distribution and Liuxian Zhang, who has worked on multiple experiments using the light source in the TEM, as well as all the other students in the Crozier group for their encouragement, and help over the years.

This work was supported financially by the US Department of Energy grant DE-SC0004954. The use of ETEM at John M. Cowley Center for High Resolution Microscopy at Arizona State University is gratefully acknowledged.

Finally, and perhaps most importantly, I would be remiss if I did not acknowledge the Creator of the world, God, who also created me, and gave me my small capacity to create, without which this project would not have even started. He has countless times encouraged, helped, and guided me in my life through His Word, and His Spirit, even in my scientific endeavors, and has consistently provided for my needs, and often even given me the desires of my heart.

TABLE OF CONTENTS

Page

CHAPTER Page

LIST OF FIGURES

Figure Page

INTRODUCTION

Motivation for the Work

The past decade has seen an increasing focus on renewable energy, with good reason. While non-renewable sources like coal and oil have provided for the vast majority of our energy needs over the past century, these resources will, by definition, one day run out (Owen, Inderwildi, and King 2010). There is also increasing concern that utilizing all the carbon-based fuels our planet has to offer may be disrupting our climate (Cox et al. 2000). Of all the sources of energy available to us, by far the most abundant and fundamental is solar energy. Apart from some forms of geothermal energy and nuclear energy, all other forms of energy on earth, including fossil fuels are derived more or less directly from the sun. The total power reaching earth from the sun is about 120,000 TW (Grätzel 2009). We need only collect, convert and transport/store a small fraction of this energy to supply global demand. Thus, many strategies for harnessing solar energy have been attempted.

The most well known, and extensively studied technique for converting solar energy is through photovoltaics (PV). PV has one significant limitation however, which severely limits its effectiveness as a standalone technology. Solar energy is not consistent at any point on the globe over time. At night, there is no power, and even in the day, there are significant fluctuations in the amount of energy that reaches the PV cell from the sun (Woyte et al. 2006). This leaves two options, either the power companies must have enough capacity through traditional sources that they can go without the extra power generated by PV, or the power

generated from the sun should be stored so that during the night, or during shady conditions, the stored energy can be used to continue supplying power. While storing electricity is routinely accomplished in our daily lives through the use of batteries and capacitors, the energy capacity of such technologies is actually quite low, and insufficient for the magnitude of energy that would need to be stored to power a city overnight (Zalba et al. 2003).

Photovoltaics is not the only technology that can be used to harvest solar energy however. While PV converts solar energy into electricity, photocatalysis converts solar energy to chemical energy. This is ideal because energy stored this way, in the chemical bonds of molecules, is quite stable, and can be easily transported across long distances. As discussed above, PV requires a separate storage technology to be a viable large scale source. Photocatalysis integrates conversion and storage into a single technology. Still, two serious drawbacks facing photocatalysis today are that significant gaps remain in our understanding and that energy conversion efficiencies are still much lower than for PV (K. Maeda 2011). This is likely in large part due to the fact that much less research has been done on photocatalysts over the past 50 years, than has been done on PV. Today, much more focus is being given to photocatalysis, and it is in the context of this broad push to understand the processes and principles governing photocatalysis that this research has been conducted.

Designing efficient photocatalysts requires an increased understanding of the link between catalyst microstructure and activity (Bell et al. 2008). To study this link in the TEM, it is ideal to be able to recreate the conditions under which the

photocatalyst will operate. Environmental TEM (ETEM) is sometimes used to study catalysts under conditions of high temperature, and reactive gas environment (Hansen 2002; Topsoe 2003; Li et al. 2004) However, the light illumination experienced by a photocatalyst during use has rarely been reproduced in-situ, leaving absent a critical experimental condition for studying light-induced processes. This research has allowed us to introduce this new stimulus into an ETEM at Arizona State University.

Context of the Work

The introduction of light into the ETEM at ASU is just the latest development pursued by researchers there to who have been studying materials in-situ for many years (Crozier, Wang, and Sharma 2008; Wang, Crozier, and Sharma 2009; Chenna and Crozier 2012; Sharma et al. 2012). Much of this work has been completed on the Tecnai F20 at Arizona State, which is equipped with a differential pumping system, allowing reactive gasses to be in contact with the sample, up to a relatively high pressure of a few Torr (Crozier and Chenna 2011) while still imaging the sample at the nanoscale. Thermal catalysts for the partial oxidation of methane have been studied (Chenna, Banerjee, and Crozier 2011; Chenna 2011) as well as materials for fuel cells, which also operate in gaseous conditions(Sharma et al. 2012; Sharma 2011). More recently the Crozier group has been studying photocatalysts, synthesizing unique nanostructures (Santra and Crozier 2011) and characterizing activities (Leyva Porras 2010). In addition to the reactor based studies, it will be beneficial to study the materials at the nano- and atomic scale as they are catalyzing a reaction in the ETEM, so a system has been designed and built to illuminate the sample *in situ*.

A few other groups around the world have pursued similar techniques to introduce light into the TEM. Recently, much effort has been put forth to develop an ultrafast imaging method. This work has introduced light into the TEM in the form of intense laser pulses, which are directed to both the electron source and to the TEM sample (T. LaGrange et al. 2006). The laser light that reaches the sample is powerful and capable of generating extreme heating conditions within the TEM (Taheri et al. 2009; Thomas LaGrange et al. 2008), but these laser systems are not

intended for experiments to study illumination effects over wide wavelength ranges. Several researchers have also focused on studying optical responses of materials in the TEM using modified sample holders (Cavalca et al. 2012; Shindo et al. 2009) to allow light to enter the microscope along the sample rod. Experiments currently published by these researchers are mainly proofs of concept, and have not yet pushed forward any scientific frontiers. At least one other group introduced the light through a separate port on the TEM column (Kenta Yoshida, Yamasaki, and Tanaka 2004a; K. Yoshida et al. 2007). However, this group has not published any research using the light since 2007. This leaves significant potential to do groundbreaking research using this technique. While both the sample holder, and alternate port approaches can work, I have chosen to introduce light through a port on the microscope, because this allows greater flexibility in selecting the sample holder used in any given experiment, since any standard sample holder may be used simultaneously with the light illumination. In this way, multiple stimuli can easily be applied in the same experiment.

Finally, it is important to note that while the current design has been tailored specifically for the Tecnai F20 environmental TEM at ASU, the light source has been intended for use in a second microscope as well. While the Tecnai has unique capabilities to observe the catalysts which drive chemical reactions at the nanoscale, the slight electronic structure changes induced in the material by the light irradiation are not observable using EELS in the Tecnai because the energy resolution is too poor. However, a new microscope is due to arrive at ASU in the coming months from NION, which will be Cs corrected, and equipped with a

monochromator, which will allow it to achieve an EELS resolution of .03 eV (Krivanek et al. 2009). This significantly increased resolution may allow probing of electronic structure changes in semiconductors due to light irradiation (Colliex 2011). Since this microscope has not yet been delivered, this aspect of the project will only be mentioned briefly here, to provide more context for the future capabilities of similar light illumination systems using this setup.

Previous Works

Illumination Through a Port on the TEM Column

The Japanese group that introduced light using a fiber to go through a port on the TEM column was led by Kenta Yoshida at Nagoya University in Japan. They claim to have irradiated the sample with a laser of intensity 10mW/cm^2 at a wavelength of 360nm. This is likely quite comparable to the intensities I would achieve with a 10nm FWHM filter at that wavelength. Little discussion of the precise design of the illumination system is given in the published literature of the group. The group produced thin films of organic hydrocarbon material deposited on a thin film of titania prepared using a laser ablation method. These were then irradiated with UV light *in situ* and observed over the course of 6 hours. The hydrocarbon was observed to degrade during UV irradiation, because lattice fringes in the underlying titania slowly became visible. It is claimed that this degradation occurred even in locations which were never exposed to the electron beam (Kenta Yoshida, Yamasaki, and Tanaka 2004a). The group also studied the same effect using EELS to try to quantify the degradation of these hydrocarbon films over time. It was observed that the carbon K edge peak intensity decreased with respect to the titanium $L^{2\text{-}3}$ edge peak over the course of 8 hours of UV illumination (Kenta Yoshida, Yamasaki, and Tanaka 2004b). During degradation of the organic film, changes in the titania film were also observed, and these changes were attributed to O^- anion radicals being pulled from the titania to oxidize the organic layer (Kenta Yoshida et al. 2006). In another experiment utilizing the UV illumination capability, gold nanoparticles were nucleated and grown on TiO_2 surfaces from solution using an ionic liquid which contained gold

cations. The nucleation was claimed to be initiated by photogenerated electrons, produced by the UV illumination which was maintained for 3 hours (K. Yoshida et al. 2007). Despite these apparently successful experiments, no more papers referencing this illumination system have been published, since 2007.

Illumination Through the TEM Sample Rod

Shindo et al also illuminated a TEM sample with laser light. A unique sample holder rod was developed based on previous work done by the same group (Murakami et al. 2006). This holder has two separately controllable piezodriving probes. In this setup, one of these probes was equipped with an optical fiber which allows a laser beam to irradiate the sample, which was an organic photoconductor. In this configuration, the laser light impinges on the sample perpendicular to the direction of the electron beam, which for a traditional TEM sample is not acceptable. However, the samples that were observed using this holder were not electron transparent, and instead of observing the sample directly, the electric potential outside the material was observed using electron holography (Shindo et al. 2009). Thus, for this application, illumination from the side of the sample is effective, though it would not be for most TEM samples.

Another researcher has very recently developed a sample holder for UV and visible light illumination (Cavalca et al. 2012). In this design, the TEM sample is bent so that it no longer sits in the horizontal plane, but is always tilted. In this way, light can enter along the holder rod axis, but still strike the surface of the TEM sample, rather than the side, as in the previous case. However, this means that the TEM sample is no longer perpendicular to the electron beam, and the

eucentric height will vary significantly with position on the sample. Two methods were attempted for guiding the light along the holder shaft. A system of 2 lenses was used in one design to focus a laser beam onto the sample, allowing very high intensities to be achieved. In the second design, an optical fiber was used instead, which allows greater simplicity when changing the light source, but achieves smaller intensities than the lens based design. Two experiments have been described using this system. First, CuO_2 nanoparticles were reduced to metallic Cu using UV illumination at a wavelength of 405nm and intensity of 6 W/cm^2 for 5 hours. The second experiment involved the photoreduction of a film of H_2PtCl_6 on the surface of a GaN:ZnO photocatalyst to produce metallic Pt nanoparticles. Control experiments were performed in each case to prove that the observed results were an effect of the light illumination rather than the electron beam.

While in each of the works just described, light was used to illuminate the TEM sample, in each case, a laser based light source was used, and in the sample rod based designs, the sample must be loaded uniquely, and other capabilities traditionally supplied by the holder, such as heating, cooling, etc. are not possible.

DESIGN GOALS AND CONSTRAINTS

The criteria over which the success of this project will be determined are simple. The microscope's performance must not be significantly degraded by the addition of the light source and fiber, meaning that a point resolution of .24nm must still be achieved in TEM. This resolution should be achieved while studying the sample in an environment of reactive gases, up to a few Torr of pressure, and while heating the sample up to 500°C. I want to achieve the highest possible intensity of light illumination on the sample, at any subset of the wavelength range 200-800nm.

The major angles from which the design of this addition to a microscope must be considered are mechanical, optical, and electron optical. Each of these general categories involves its own set of constraints, and all must be addressed for the addition to be viable.

Optical Considerations

The first question that must be addressed is: how will the light be directed to the TEM sample? At least two basic approaches are possible; light may be focused and directed by traditional optics such as lenses and mirrors to the TEM sample at the optic axis of the microscope, or the light may be guided there using an optical fiber. A method using lenses requires that the light source be rigidly attached to the microscope, while using optical fiber allows greater flexibility and simplicity since the source can be positioned anywhere in the room. The method using lenses was not attempted for this project, and so will be given no more

consideration. Instead, the method of using a fiber to direct the light will be considered in detail.

The first optical consideration is the spatial distribution of the light hitting the sample. First, it is essential that whatever the distribution may be, it should be well-characterized outside the microscope, because it is difficult to characterize the light's distribution while the microscope is being used. Knowing the distribution as well as the power that enters the optical fiber, it is possible to determine the intensity striking the sample at the electron beam position. Second, it is desirable for the light to be focused to a small spot on the sample so that high intensities can be achieved, even at moderate beam power. This desire for high intensity with low power necessitates that the source of the light be a bright source. Basic optics dictates that if the light does not originate from a small spot in the light source, it will never be focused back to a small spot on the sample. It is also essential, since a large wavelength range is used, that the optical components introduce as little chromatic aberration as possible, and be suitable for the UV, visible and near IR range. The high intensities produced in this way are useful for studying materials under extreme conditions, and allow for studies of solar energy materials under conditions similar to concentrated sunlight schemes.

Precisely defining the spectral distribution of the light source is also essential. For some solar applications it might be advantageous to utilize a broadband light source which closely mimics the sun's spectrum. For other applications, and for many fundamental science experiments, it is useful to use a narrow range of

incident wavelengths/energies, in order to isolate the effect of photons of a particular energy, for example, above or below the bandgap of a semiconductor. The available spectrum should range from the UV (200nm) up through the entire visible spectrum. Ideally, it would be possible to also choose to transmit any subset of this full spectrum, while blocking the rest from reaching the sample.

Mechanical Considerations

There are two basic routes for guiding light to the sample area of the microscope using an optical fiber. The fiber may be threaded along the sample rod, or it can be introduced through another port on the side of the column. Using a specially designed sample rod to introduce light becomes a problem however, if the user of the microscope wants to use other commercially available holders to simultaneously introduce another capability to the microscope, such as heating, cooling, or electrical/mechanical measurements/stimuli.

Getting a fiber tip close to the sample, after going through a port on the column is non-trivial however, because space in the column is limited, especially in the pole piece gap, and optical fibers may not be bent to radii smaller than a certain value without significant optical losses. The port itself can also be a spatial limiter, because, for example, the diameter of the ports on the Tecnai F20 for which the current system is being designed is just over 25mm. These limitations are shown to scale in Figure 2.1. A further limitation may be introduced by individual holders. The heating holder currently used in the Tecnai F20 at Arizona State University is 2.4mm thick, with an inner diameter of 3.4mm as shown in Figure 2.1. Because of this, care must be taken to position the end of the fiber such that

the walls of the furnace in the heating holder do not cast a shadow onto the sample area. This is quite an extreme case, and usually, sample holders are much shallower, allowing the light to illuminate the sample, without any shadowing. It is also essential that the tip of the fiber not touch the sample holder when the sample is tilted, because the tip may be damaged or misaligned by such contact.

Any system for introducing a fiber into the microscope must be able to align this fiber with a good degree of precision. It has been found, using MATLAB calculations as well as optical measurements described in the Ex Situ Spatial Characterization 40section of Chapter 4) that for this system, the fiber position should be set to within 200μm of the ideal position, or the intensity will be significantly changed at the optic axis position on the sample (see Figure 4.9). In addition to precise alignment, it is advantageous in such a system, to be able to retract the fiber from its functional position, to protect the fiber when it is not being used, without removing the fiber completely from the microscope. Thus, a large amount of travel in the axial direction is needed, in addition to the fine control used for proper alignment.

Electron Optical Considerations

Constraints also arise in the design process due to the effects of the addition to the electron optical performance of the microscope, which must not be degraded. Vibrations produced by the light source need to be monitored, to ensure that these are not transmitted to the sample, degrading the resolution of the microscope. Magnetic interference is potentially an even greater threat to the microscope's performance, and thus, all materials which enter the TEM column should be non-

magnetic. Electrostatic fields near the sample can also cause problems, if the end of the fiber charges due to backscattered and secondary electrons from the sample; this must be considered in the design of the fiber tip.

Environmental Considerations

Finally, the design must take into account the environment to which the components within the microscope vacuum will be subject. All components inside the vacuum system of the microscope clearly must be vacuum compatible, having low vapor pressures. Ideally, these components should also be easily pumped out, and for example, all threaded bolts should be vented. Because the microscope is an environmental TEM and reactive gasses are often introduced into the sample chamber, it is also important that the materials used be resistant to attack by the gases commonly used in the Tecnai. These gases include H2, O2, and CO. Thus, metals that are not easily oxidized and ceramics that are not easily reduced are preferred. Some *in situ* experiments also involve heating the sample to high temperatures, and while under high vacuum conditions there is no conduction path from the sample to the fiber tip, radiative heating of the tip will occur, as well as some conduction if gases are also present. Thus, it is also important that the fiber tip be able to withstand elevated temperatures up to a few hundred degrees Celsius.

Figure 2.1 Geometrical Limitations

The space available for the fiber optic inside the microscope is quite limited. The port through which the fiber and supports must pass is small, and the pole pieces of the TEM introduce serious limitations on the angle at which the fiber can approach the sample Finally, the heating holder shown with dimensions necessitates that the light come in at a steep angle.

DESIGN IMPLEMENTATION

A diagram showing the entire system described below is given in Figure 3.1.

Light Source

The light source employed in the present design is an Energetiq EQ-99 laser powered broadband light source, shown in Figure 3.2. This is essentially a xenon lamp, but powered by an IR laser rather than an electric discharge. This broadband source is preferred in the current design rather than a series of lasers or other narrow sources, though laser sources could still be used in this system if desired. The advantage to using a broadband source is that it can more easily simulate the natural irradiation of the sun (see Figure 3.3) for solar energy based applications, and a single source simplifies the design and keeps costs down. The chosen light source is also bright; the diameter of the source is approximately 100µm. This allows the light to be focused onto a 600µm core fiber with minimal loss. Since the light then exits from this 600µm fiber near the TEM sample, the light spot can be quite small, and thus the intensity correspondingly high. Energetiq produce several light source models, and the EQ-99 was specifically chosen because it was thought that the light from this source would be easiest to focus back to a point. The total power output by the light source is quoted to be 800mW.

Pre-Fiber Optics

Focusing the light emitted from the source onto a 600µm fiber is accomplished by the use of two off-axis parabolic mirrors, shown in Figure 3.4. No lenses are used, as these introduce chromatic aberrations, which are undesirable, since the light source emits over a large wavelength range; mirrors do not introduce significant chromatic aberration. The first mirror, which can be positioned relative to the light source using 3 micrometers, collimates the rays emitted from the focal point into a parallel beam. This parallel beam is then incident on the second mirror which focuses the collimated light back to a second focal point, where the fiber tip may be precisely positioned using a 3 axis positioner which connects with the fiber via an SMA connector. Between the second mirror and the focal point where the fiber end must be positioned, several optical components are positioned, as shown in Figure 3.4. An aperture for reducing the beam intensity is included here. More importantly, a 1 inch diameter filter is also introduced, allowing the spectral range of the light to be modified. This filter can be easily interchanged, with the light source powered up, by unscrewing the section of optics containing the aperture and fiber positioner, and long pass, short pass, or band pass filters may be used. The filter to be used is dependent on the material being studied and the nature of the individual experiment. In future iterations of the design, tunable filters, which change their pass band based on the angle at which light is incident, may also be incorporated. In this way, a small number of filters would allow for a narrow band at any wavelength to be specified. The spectra resulting from the light source, the optical components of the system, and a selection of filters has

been calculated from the various manufacturers' spectra and is shown in Figure 3.5

Optics Alignment

All of these optics must be correctly aligned to ensure that a minimum amount of light is lost in the optical system. First, the light source must be aligned with respect to the first parabolic mirror. The light is essentially a point source, so this point should be positioned at the focus of the paraboloid. This is accomplished using a 3 axis manual translation stage which connects the light source to the mirror housing. This setup was constructed by Energetiq, the manufacturer of the light source. It should be noted that the company did not construct this properly, and a modification was made to improve the alignment, as is described in Appendix A. To complete rough alignment of the light source, the optics past the filter are removed and the shape of the light beam is observed simply by placing a paper in the beam, and adjusting the micrometers of the translation stage so that the beam is round. The two parabolic mirrors are fixed with respect to one another, and are already aligned. The fiber however, can be moved with respect to the mirrors, via a 3 axis lens tube manipulator from Thorlabs. With the fiber attached to this manipulator, and the other end fixed to illuminate a photodetector, it is possible to do fine alignment of the light source by observing the voltage produced by the detector while adjusting the micrometers. Finally the fiber manipulator can be adjusted to maximize the voltage, which indicates that the maximum possible light is passing through the fiber.

Optical Fibers

Two fibers are used in the current design. The first is a standard 2m long, 600 μm silica core, silica clad high OH solarization resistant fiber assembly, from Ocean Optics which gives high UV transmittance and durability. The fiber runs from the focal point of the second parabolic mirror to the fiber feed through flange mounted on the microscope. This flange allows light to pass into the second fiber which is within the high vacuum of the microscope. Both fibers are attached to the feedthrough by SMA connectors.

This second fiber inside the TEM was specially ordered from Ocean Optics; it also has a 600 μm core diameter, with silica cladding, but rather than the standard polymer-based protective buffer and jacket, it is protected only by an aluminum buffer, as shown in Figure 3.6. This aluminum buffer fulfills many of the design criteria for the fiber; the aluminum is conductive, so that the tip does not charge up when scattered and secondary electrons from the sample hit the fiber tip, and also ensures that the buffer does not outgas or degrade in vacuum or reactive gasses, as a polymer might. It is also non-magnetic, which is necessary to avoid interference with the powerful magnetic field of the microscope's objective lens, and the metal can be heated to several hundred degrees Celsius without deformation.

In addition to being specially fabricated, the aluminum buffered fiber is also uniquely positioned and cut to be 22.67cm long; this is shown in Figure 3.7. The optical fiber used in this design should be bent to a radius no smaller than 25cm or the light transmission along the fiber will be reduced. Because of this restriction,

as well as the limit imposed by the 2.5cm diameter microscope port through which the curved fiber must pass, the largest possible angle that the fiber tip can make with the horizontal is about 15°, since only the bottom 1.25 cm of a 25cm circle may be used to construct the curve leading up to the sample. The curve seen in Figure 3.7 conforms to this 25cm radius constraint, and fits within the microscope port, while bringing the fiber to this maximum angle. The fiber itself is flexible, and so to maintain the fiber's contour along this path, a brass tube is used. Because the inner diameter of the tube is quite small, it has been equipped with a small funnel shaped attachment on one end for easy insertion of the fiber, and has a cap on the other end which fits around the fiber snuggly to securely position the fiber tip, as shown in Figure 3.8. Like the aluminum, brass is non-magnetic and conducting, and reasonably robust chemically. The tube is itself held in place by three aluminum support rods, which are bolted to a flange that connects to the fiber feed through. This is shown in Figure 3.9.

One end of this specialized fiber is terminated by a standard SMA connector, which connects to the high vacuum side of the feed through flange, while the fiber end near the sample has no connector, and is cut at a 30° angle. This cut is essential to the entire design, since, with the maximum fiber angle of 15° shown in Figure 3.7, the light could not be directed to the sample center in any other way, due to the demanding spatial constraints earlier described and shown in Figure 2.1. With the cut, the light is easily directed onto the sample, and is not blocked by the walls of the heating holder used in the microscope. This is shown schematically in Figure 3.10 .

Fiber Manipulator

Finally, the fiber is precisely positioned relative to the microscope through the use of a manipulation stage which is shown schematically in Figure 3.9. This manipulator was designed using CAD software and built specifically for this project, and the design is original. The movement of the fiber is facilitated by a bellows, which is appropriately connected to the microscope on one end, and to the fiber feedthrough flange on the other. This movement is controlled by micrometers and springs in each of the three Cartesian directions with about 3mm of travel. None of the micrometers are firmly attached to the components they move, so springs are used to maintain contact with the micrometers. The movement is limited in a unique way, using a captive ring attached to the flange at the free end of the bellows. This ring can float in the two dimensions perpendicular to the fiber in a fitted cavity to prevent it from tilting. This entire assembly is spring loaded in a round aluminum can which is 5 inches in diameter, and allows for the motion in the direction of the fiber. All this is shown in Figure 3.11. Also incorporated into the manipulator design is the capability to retract the fiber, guide tube, and support rods away from the center of the microscope by about 1.5cm, a distance much greater than that afforded by the micrometers used. Retracting the fiber this far minimizes the danger of striking the pole pieces with the fiber or supporting rods when the apparatus is attached or detached from the TEM column. It also allows the entire apparatus to remain attached to the microscope, while keeping the fiber tip far from the sample area when TEM users are not utilizing the light source in their experiments. Finally, as seen in Figure 3.11, lead shielding is appropriately located in the design close to the fiber tip to

ensure that x-rays emitted from the sample are blocked from leaving the microscope.

Unfortunately the fiber manipulator does not work as well as intended. While the fiber is not meant to tilt in any direction, in practice, some tilting is inevitable, and this complicates the alignment procedure. Since the fiber exits the manipulator in the center, the micrometers used to push the fiber in toward the microscope are placed symmetrically on either side of center, so if these 2 are not moved by precisely the same amount at all times, the fiber is tilted. This does not prevent proper positioning of the fiber, but does make it more difficult. A second known issue is that the springs which act perpendicular to the fiber direction, working against the micrometers, do not have enough force to allow the full range of movement that was intended. Again, this is not a critical problem, and alignment can still be achieved, but it could be made better by incorporating stiffer springs.

Modeling Emitted Light from the Fiber Tip

The process of designing the fiber that illuminates the sample was shortened considerably through the use of modeling before any physical components were purchased. This modeling was done using both CAD software and MATLAB. The CAD software used is called CADKEY which is no longer on the market, but can be imported into currently supported software like Solidworks. Using CAD, it was possible to model all the dimensions of the TEM, including the pole pieces and the sample holder, as well as the fiber and its supports. Many of the figures presented in this thesis are based on these CAD models. The light cone produced

by a normally cut fiber tip is symmetric, and simply defined by the numerical aperture of the fiber, but a fiber cut at an angle requires more careful consideration. CAD software also simplified the calculation of the angles at which light from the fiber would exit a cut tip, as seen in Figure 3.7 and Figure 3.10.

Basically, the refraction at the cut surface of the fiber on either end is calculated using Snell's Law, which states:

$$\boldsymbol{n_2 \sin(\beta_2) = n_1 \sin(\beta_1)} \tag{3.1}$$

Inside the fiber, there is a maximum transmission angle, θ_2, beyond which light no longer undergoes total internal reflection in the fiber. This angle can be determined by Snell's Law, from the numerical aperture of the fiber, which specifies the maximum angle θ_1 at which light entering the fiber will be transmitted, and the refractive index of the fiber core, n_2. This is shown in Figure 3.12. Rearranging Eq 3.1 gives:

$$\boldsymbol{\beta_2 = \operatorname{asin}\left(\frac{n_1}{n_2}\sin(\beta_1)\right)} \tag{3.2}$$

Plugging in the numbers and using the symbols used in Figure 3.12, we have:

$$\boldsymbol{\theta_2 = \operatorname{asin}\left(\frac{1}{1.47}\sin(12.7°)\right) = 8.6°} \tag{3.3}$$

Using CAD, it is easy to keep track of all the angles between the light rays and the fiber cut surface and walls. The angle between the cut fiber end, and this maximally angled transmitted light ray is then: $\alpha + \theta_2$, as shown in Figure 3.12. Using the same procedure as for the light entering the fiber, we get Snell's Law to be:

$$n_2 \sin(\alpha + \theta_2) = n_1 \sin(\theta_3 + \alpha) \quad (3.4)$$

Rearranging, plugging in numbers, and solving yields:

$$\theta_3 = \sin^{-1}(1.47 \sin(30° + 8.6°)) - 30° = 36.5° \quad (3.5)$$

An identical calculation can be performed for a light ray entering the fiber from the opposite extreme angle of -12.7°. These two together yield the limits of the light cone that exits the fiber, as shown in Figure 3.7.

This basic calculation only defines the maximum angles to which the light will be bent as it exits the fiber tip. However, it is important for the design of the fiber to know also where the maximum intensity will be on the sample, as a function of all the available design parameters, such as fiber tip cut angle, and tip position relative to the sample. To determine this, without going through many physical iterations of the design, a MATLAB code was written which calculated the expected light intensity at every point on the TEM sample, based on the position, cut and refractive index of the fiber. The details of this much more involved calculation, as well as the MATLAB code itself are included in Appendix B. Some results of this code are shown in Figure 3.13 where the position of the fiber is varied relative to the sample. Unfortunately, after the fiber was purchased it was found that, while the peak position was close to correct, the shape of the measured distribution did not match well with the MATLAB calculated distribution, as shown in Figure 3.14. This discrepancy was never resolved. Despite this, the MATLAB code proved invaluable in the initial design of the fiber before any prototypes were produced.

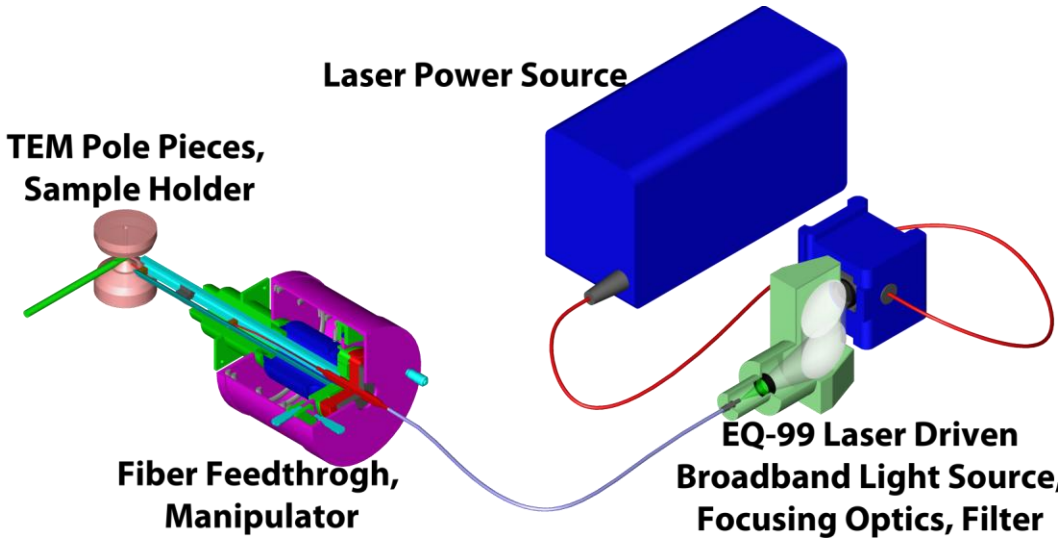

Figure 3.1 Design Overview

This diagram shows the entire system which is used to illuminate the TEM sample *in situ*. An infrared laser powers the broadband light source. The light from this source is focussed by 2 parabolic mirrors (white) and passes through a filter (green) before entering a fiber optic cable (blue). This is connected to a feedthrough (red) and this is connected to the microscope by a manipulator which allows the fiber tip to be precisely aligned with respect to the sample holder, which sits between the pole pieces of the TEM.

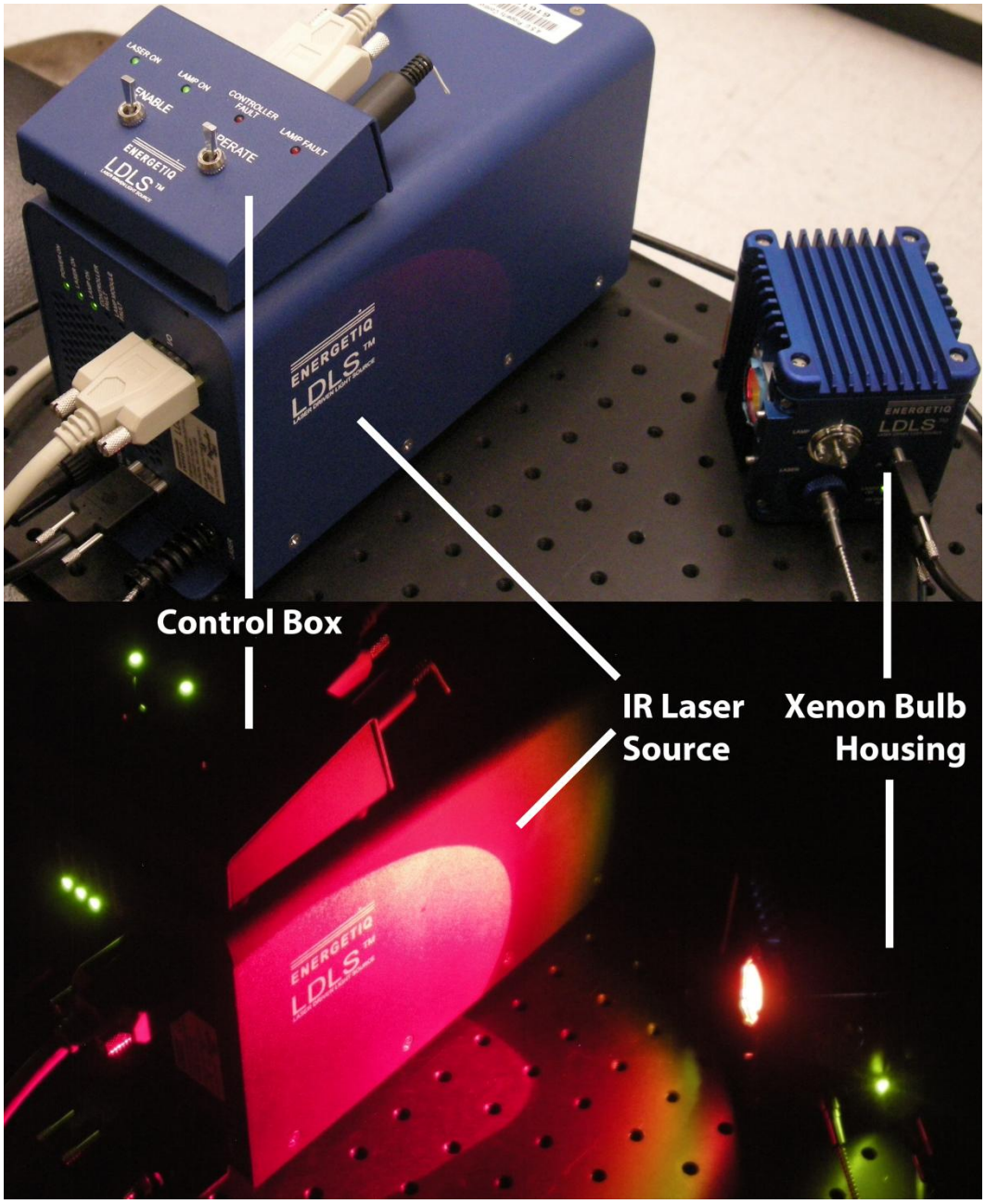

Figure 3.2 Laser Driven Light Source

Photos of the EQ-99 laser driven light source by Energetiq, showing the control box, infrared laser source and the light housing; the focusing optics are not attached. The bottom photo is taken from an identical angle as the top one, but with the lab lights off, so that the light source (red filtered) illuminates the setup.

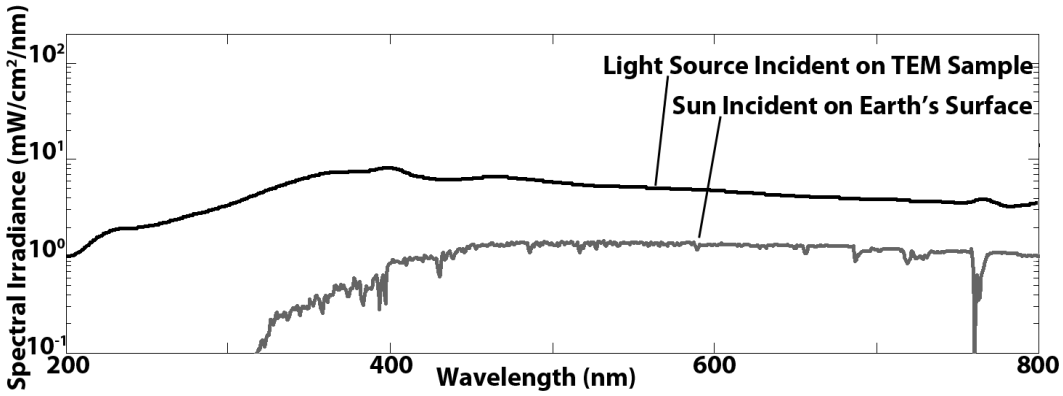

Figure 3.3 Light Source Spectrum

The spectral irradiance (intensity per unit wavelength) of the light that reaches the sample at the electron beam location (black). This spectrum includes the losses associated with all of the optical components. The intensity that reaches the TEM sample is about 10x that of the AM1.5 solar spectrum which is also shown (grey) in the visible range. The light distribution is reasonably similar to the solar spectrum over this range. The light source also has significant intensity in the UV portion of the spectrum, allowing excitation of semiconductors with bandgaps up to about 6eV. This intensity is for a sample that is untilted; tilting the sample to be normal to the light beam emitted by the fiber tip, will increase the intensity by about 20%, as shown in Figure 2.1.

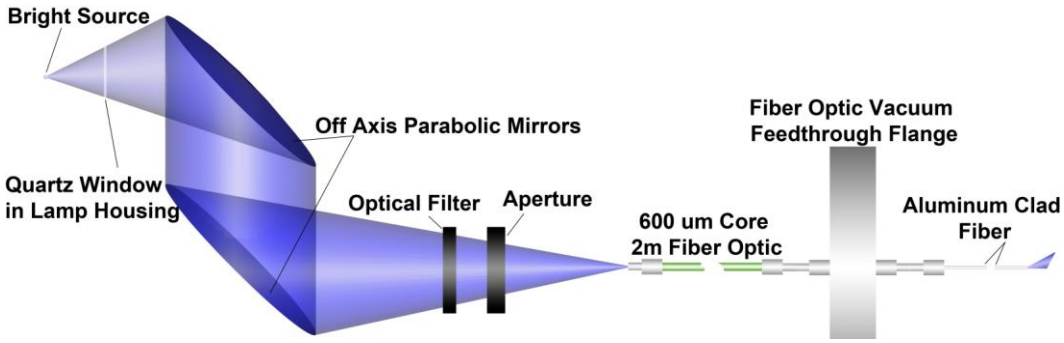

Figure 3.4 Optical Path

A scale diagram showing the path that light travels from the point source to the sample. The light (colored blue) from the bright, broad spectrum source passes through a quartz window on the light source housing, then is focused back to a small spot using 2 off-axis parabolic mirrors, rather than lenses to reduce chromatic aberrations. The light also passes through an optical filter, and an aperture for controlling the spectrum before entering an optical fiber. A fiber optic vacuum feedthrough flange allows the light to enter into the high vacuum of the microscope, where it continues toward the sample within a custom 600µm silica core, aluminum clad fiber which is cut at an angle, so the light beam is bent up toward the sample. All fiber connectors are SMA.

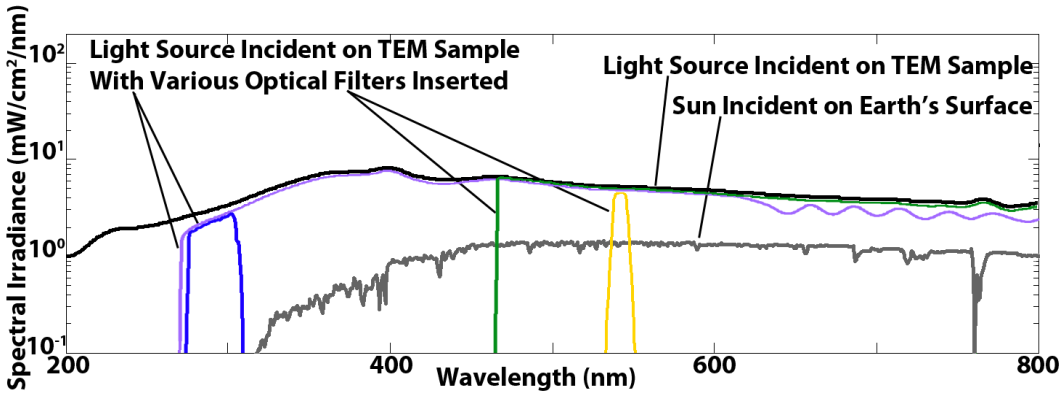

Figure 3.5 Light Source Spcetrum with Filters

This plot shows the same spectra as Figure 3.3 but includes spectra that result from inserting optical filters as well. The filters shown here are for illustration only, and while they are commercially available, not all the filters shown have actually been purchased for this project.

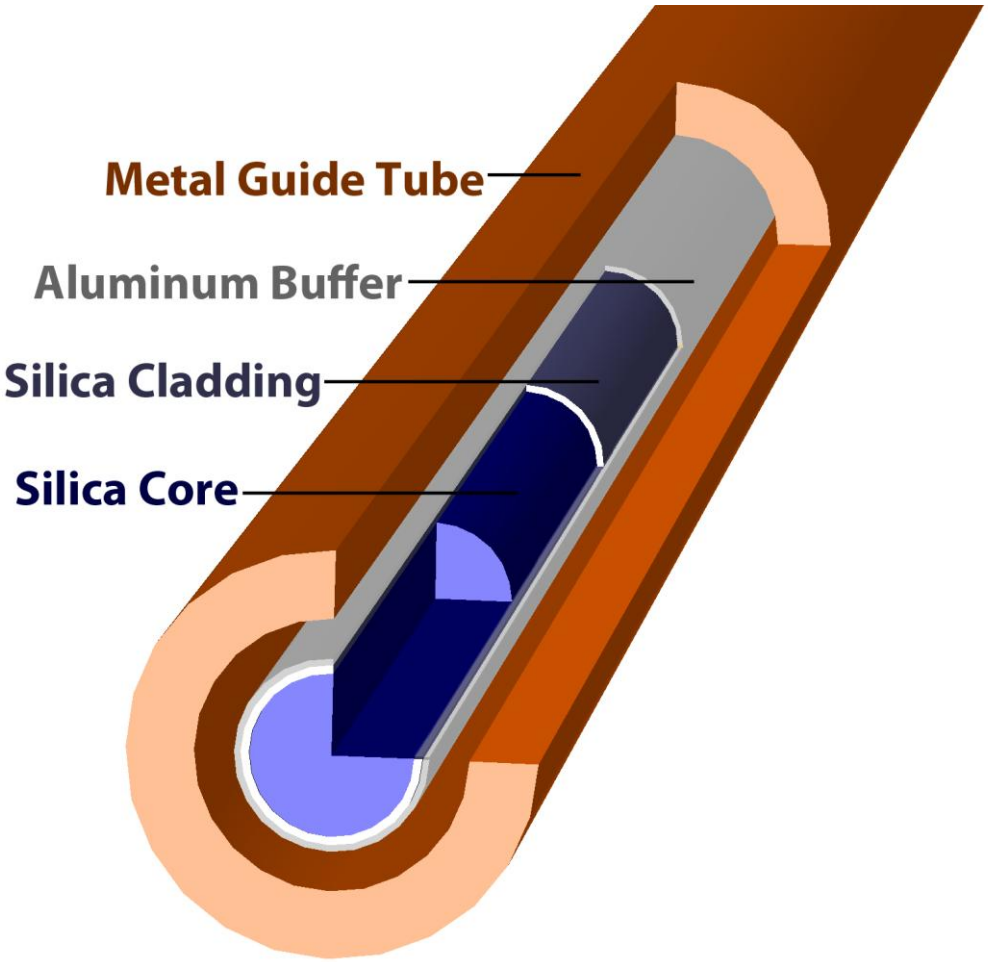

Figure 3.6 Custom Fiber.

To scale cutaway diagram showing the custom fiber inside the microscope. The fiber has a silica core where the light travels, a silica cladding, with a different refractive index, which causes the total internal reflection in the fiber. It also has a buffer of aluminum, which makes the fiber elctrically and thermally conductive, but not magnetic. The fiber does not have a jacket, but is guided to the sample position by a brass guide tube.

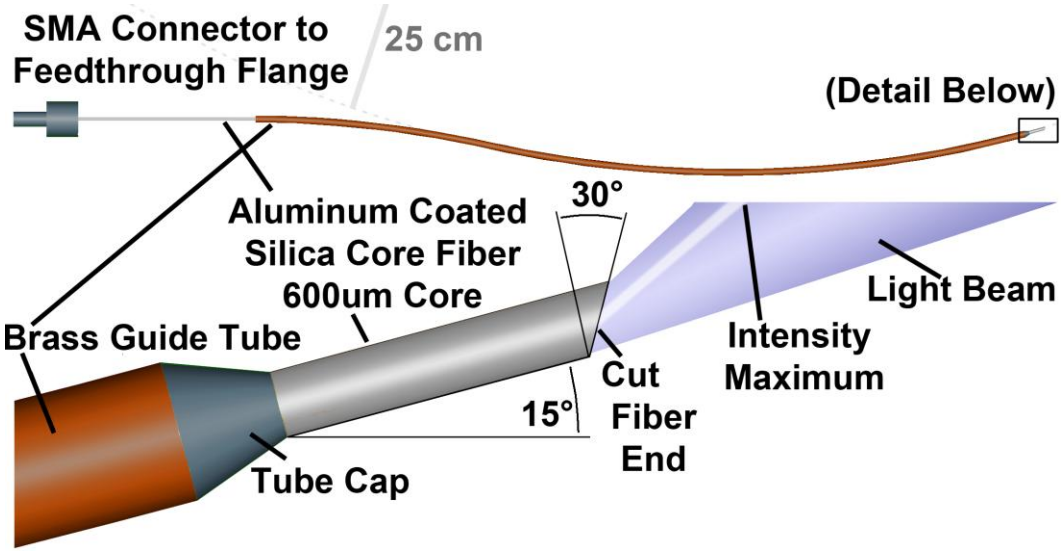

Figure 3.7 Custom Fiber Detail.

The custom fiber which sits inside the microscope vacuum is shown to scale here. The 25cm radius bend in the fiber is the maximum allowable without optical loss, and is maintained using a brass guide tube, with a tight-fitting cap to hold the fiber in place. This gives a 15° angle with the horizontal at the tip. To produce a beam which will illuminate the TEM sample, the fiber end is cut at 30°, yielding the beam shape shown. The angles here were calculated using CAD and basic optics.

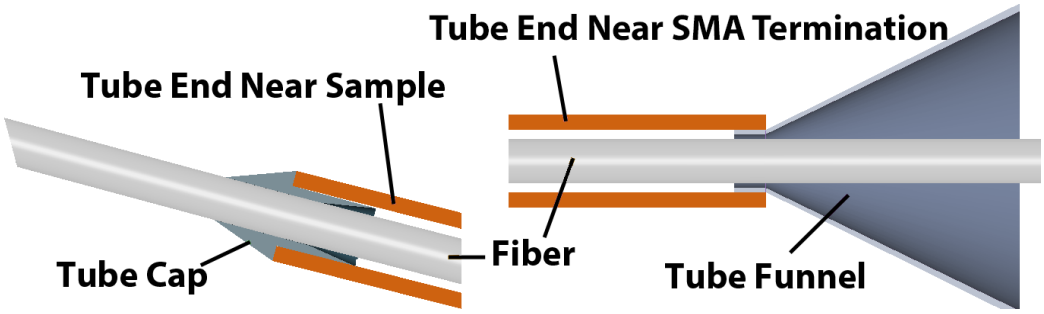

Figure 3.8 Fiber Guide Tube Details

The two ends of the brass fiber guide tube are terminated by aluminum fixtures. On the end near the fiber tip, a cap is threaded into the brass tube. The inner surface of this cap fits closely around the aluminum buffered fiber, to securely hold it in place. The opposite end of the guide tube is fitted with an aluminum funnel that makes it easy to insert the fiber tip into the brass tube, which is quite small.

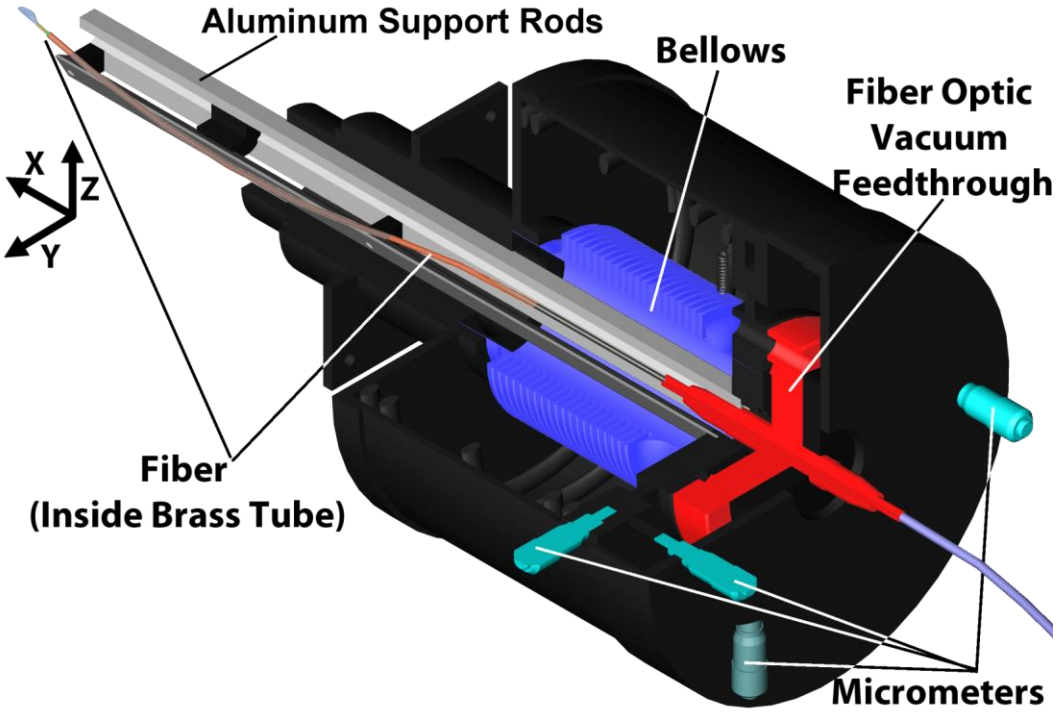

Figure 3.9 Fiber Manipulator

The fiber tip is positioned using this apparatus. The brass guide tube is supported by three support rods (light grey) which are attached to the vacuum feedthrough (red). The feedthrough is positioned using micrometers (light blue), and the movement is facilitated by a bellows (dark blue). All other components are not colored to emphasize only these few key features.

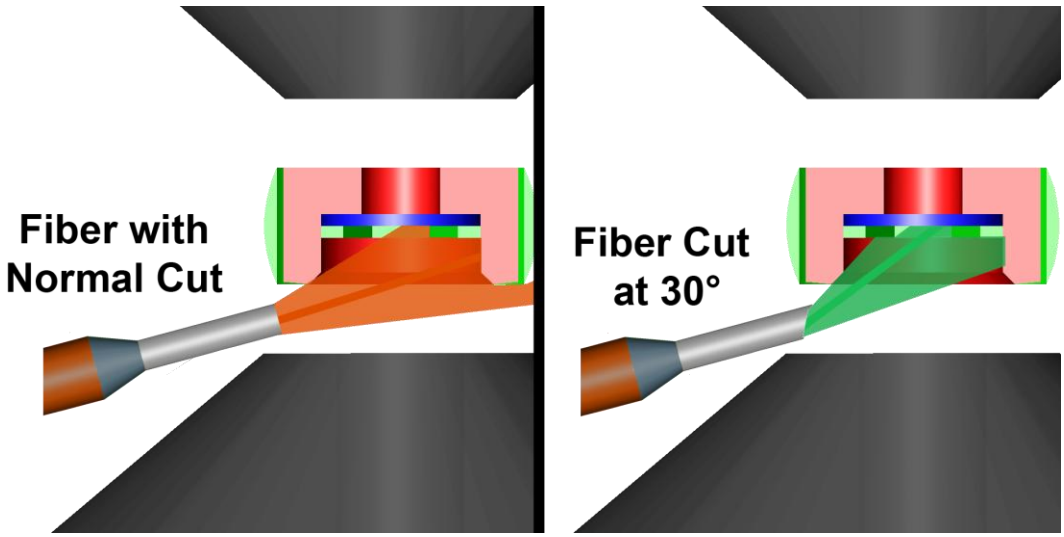

Figure 3.10 Fiber Beam Comparison

With the fiber tip in an identical position the normally cut fiber does not illuminate the sample much. The maximum intensity is not on the sample, while in the case of the 30° cut fiber, the maximum intensity falls directly on the center of the sample. In fact, using this heating holder, and the standard fiber, it is not possible to position the tip such that the maximum reaches the sample, because the holder casts a shadow onto the sample. Thus, the 30° cut is critical to the entire design.

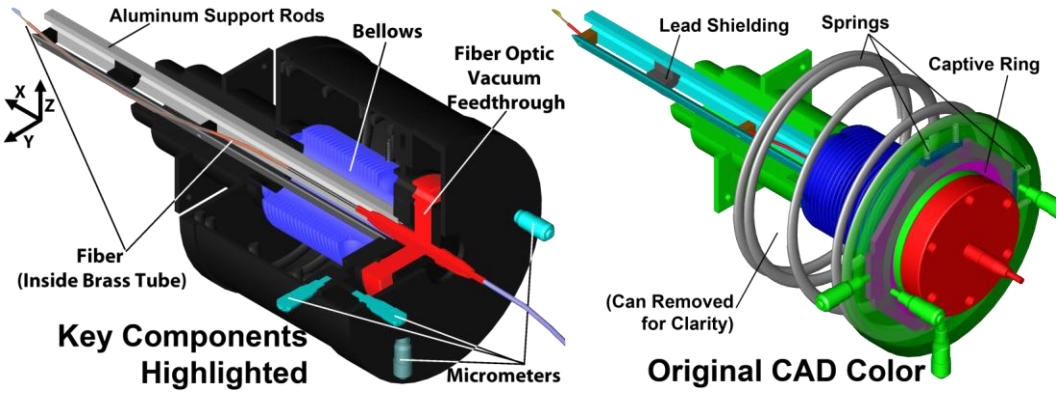

Figure 3.11 Fiber Manipulator CAD Color

The same diagram of the manipulator as in Figure 3.9 is shown here, side by side with another view of the same CAD model in the original CAD colors, but without the outer aluminum can, and with some parts shown partially transparent. This allows a better view of the mechanism that constrains the movement of the fiber. A captive ring sits inside a close fitting holder. This ring is pushed by the micrometers and springs. The lead shielding that is required to absorb X-rays emitted from the sample area for safety is also labeled.

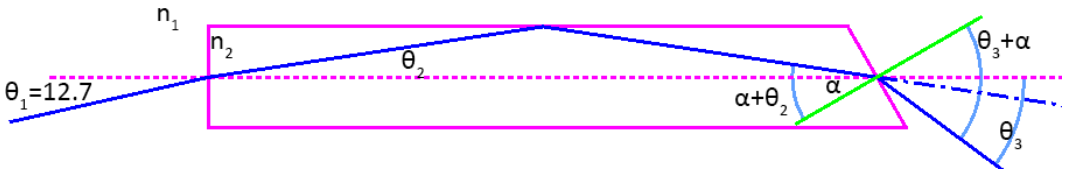

Figure 0.1 Cut Fiber Light Cone Angles

The angles relevant to calculating the direction of the light out of the angled-cut fiber. The light entering the fiber at the maximum angle of 12.7° from the fiber axis will exit the fiber at an angle of θ_3 with respect to the fiber axis. The fiber cut angle α, defined between the cut surface normal and the fiber axis, is 30°. The calculation of θ_2 and θ_3 is given in the text.

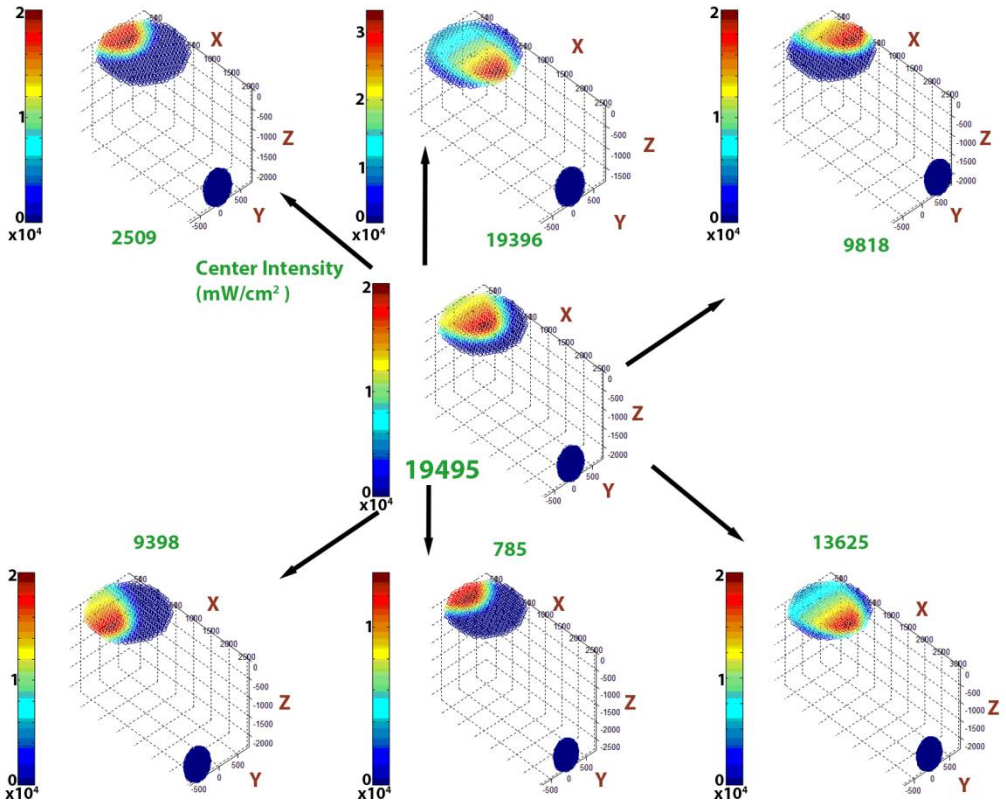

Figure 3.13 MATLAB Calculated Intensities

The calculated intensity distributions on the TEM sample for a series of fiber positions. The colorbars give the intensity in units of mW/cm^2. The ideal position is shown in the center of the figure. From there each of the other plots give the distribution if the fiber is moved 500μm in that direction The green text gives the expected intensity at the center of the sample in mW/cm^2.

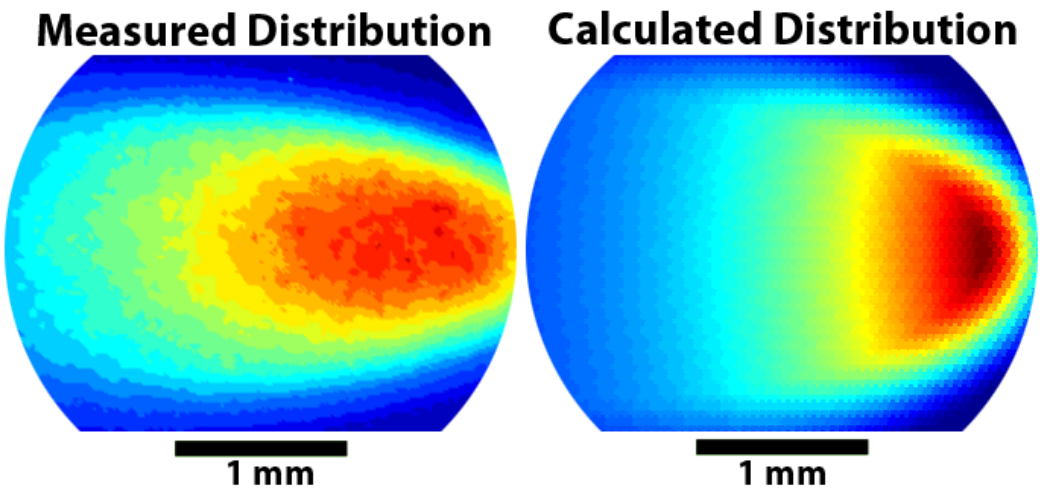

Figure 3.14 Measured vs Calculated Distributions

The spatial light intensity distribution calculated in MATLAB is compared to the experiemental distribution measured using an optical microscope. While the size of the actual distribution is close to the caclulated one, the shape is clearly different. The reasons for this discrepancy are not fully understood.

CHARACTERIZATION OF CURRENT CAPABILITIES

Spectra

As mentioned earlier, and shown in Figure 3.3, the light source used to illuminate the TEM samples is a broadband source, with significant intensity at wavelengths from around 200nm to over 800nm. The spectrum that has been given is the one provided by Energetiq, the manufacturer of the light source. It is a typical xenon lamp spectrum, and is approximately a blackbody spectrum, as shown in Figure 4.1, where it is fit by a blackbody curve with a temperature of 7000C However, this spectrum is not the one that reaches the TEM sample. As the light is reflected by mirrors, and transmitted through fibers, and the fiber feedthrough, the spectrum is modified slightly. Any filter used will of course also change the spectrum dramatically. The resulting spectrum can be easily calculated by multiplying the transmittance (or reflectance in the case of the mirrors) spectra together with the original spectrum. This yields the spectrum given in Figure 3.5, which gives both the unfiltered spectrum as well as the spectra with several filters inserted. The composite spectrum of the optical components, without any filters is shown in Figure 4.2. From this spectrum it is clear that a significant percentage of the power emitted from the light source will not reach the TEM sample due to imperfect optical components.

As mentioned earlier, it is important in many applications to use a certain subset of the full spectral range available with this light source. This may be a specified wavelength, or it may be a large range, like all the visible spectrum, or only the UV. Such a range may be selected from the broadband spectrum using optical

filters. Filters come in 4 basic categories: bandpass, notch, longpass and shortpass. Bandpass filters transmit a specified, and usually small range of wavelengths, while notch filters transmit most wavelengths but block a small range. Three bandpass filters were bought for this project from Thorlabs and their spectra are shown in Figure 4.3. Longpass (shortpass) filters transmit wavelengths longer (shorter) than some cutoff wavelength. Two longpass filters were bought for the project, specifically corresponding to below and above the bandgap of Titania. Their spectra are also given in Figure 4.3.

Measuring Intensities

Several light intensity measurements have already been given in this document, which have a significant bearing on the success of this project, since a high intensity is desired. More quantitative measurements are described in this chapter, so, it will be advantageous to precisely describe the methods used to make these intensity measurements, as this is not as simple as it might seem. The intensity of any light source varies over the range of wavelengths it emits, and thus, the total intensity of the light is a sum of the intensities at each wavelength. Further complicating the problem of measuring intensity, any given detector also detects each wavelength with a different efficiency, and the "spectrum" of this variation is called the response function of the detector. These considerations complicate measurement of overall light intensities.

For the work, two detectors were used. One is a biased photodiode detector produced by Thorlabs: the DET10A, which is fitted with a variable resistance resistor, set to 50,000Ω. The other detector is also a photodiode, but unbiased, and this diode is

the one incorporated into a TEM sample rod, for doing in-situ measurements. For the purpose of this project, I have called the in-situ, unbiased diode the "photodiode", and the ex-situ detector by Thorlabs, the "photodetector." The output of the biased detector is a voltage, usually measured in mV. This voltage is directly proportional to the intensity (mW/cm^2) falling on the photodiode surface, but the constant of proportionality is dependent on several factors. The spectrum of the light, the resistance setting of the variable resistor, and the response function and area of the detector all affect the proportionality constant, which will be derived here. The voltage that is measured from the detector can be given by the expression:

$$\mathbf{V} = \boldsymbol{\rho} \int \mathbf{A} * \mathbf{R}(\boldsymbol{\lambda}) * \mathbf{P}(\boldsymbol{\lambda}) \mathbf{d}\boldsymbol{\lambda} \tag{4.1}$$

Where V is the measured voltage (V), ρ is the resistance of variable resistor (V/A), A is the detector area (cm^2), $R(\lambda)$ is the spectral responsivity (A/W), and $P(\lambda)$ is the spectral power density ($W/cm^2/nm$). The limits on the integral should be over the entire range that the detector functions. In this case the range was chosen to be from 200 to 1100nm. The spectral power density can be normalized so that the integral over the this range is equal to 1. This allows the spectral power density $P(\lambda)$ to be broken up into 2 components, one that is wavelength dependent: the normalized spectral power density p (nm^{-1}), and one that is a scalar value: the intensity W (W/cm^2) such that:

$$\mathbf{W} * \mathbf{p}(\boldsymbol{\lambda}) = \mathbf{P}(\boldsymbol{\lambda}) \tag{4.2}$$

These two equations together yield:

$$\mathbf{V} = \boldsymbol{\rho}\int \mathbf{A} * \mathbf{R}(\boldsymbol{\lambda}) * \mathbf{W} * \mathbf{p}(\boldsymbol{\lambda})\mathbf{d}\boldsymbol{\lambda} \quad 4.3$$

Since W and A are constants with no λ dependence they can be pulled out of the integral, and the equation can then be written as:

$$\mathbf{V} = \mathbf{W} * \left(\boldsymbol{\rho}\mathbf{A}\int \mathbf{R}(\boldsymbol{\lambda}) * \mathbf{p}(\boldsymbol{\lambda})\mathbf{d}\boldsymbol{\lambda}\right) \quad 4.4$$

Now the expression in the parentheses is a conversion factor from an intensity, W, to a voltage, V. The reciprocal of this then, which I will call C_I, is the desired conversion factor which will convert the voltage measured from the photodetector to a total intensity over the entire wavelength range.

$$\mathbf{W} = \mathbf{V}\frac{\mathbf{1}}{\left(\boldsymbol{\rho}\mathbf{A}\int \mathbf{R}(\boldsymbol{\lambda})*\mathbf{p}(\boldsymbol{\lambda})\mathbf{d}\boldsymbol{\lambda}\right)} = \boldsymbol{V} * \boldsymbol{C_I} \quad 4.5$$

The spectral power density, $P(\lambda)$, at any wavelength may be recovered simply by multiplying this total intensity, W, by the normalized spectral power density, $p(\lambda)$. Since this factor, C_I, depends on the light spectrum, a new factor must be calculated for each filter used, as well as for each optical configuration in which any optical component is removed or added. Since this calculation is often needed, a MATLAB code was written which computes a composite spectrum for any series of optical elements, and performs the necessary numerical integrations of the resulting spectrum and the response function of the photodetector to output the required conversion factor. This code is given in Appendix C

Once the conversion factor for a given optical setup and filter is known, it is simple to convert the voltage from the detector into an intensity. which is usually the desired quantity. If the spatial distribution of intensities is known as well as

the intensity maximum then the total power output by the fiber can also be determined by an integration over the illuminated area.

Ex-Situ Spatial Characterization of Light

Outside the TEM, an optical microscope was used to characterize the intensity distribution of the fiber output. The fiber manipulator was set up to illuminate a small translucent screen which was observed using a Lumenera Infinity-2 microscope. The setup for these measurements is shown in Figure 4.4. The screen was moved with respect to the fiber, to characterize the distribution at a series of distances from the fiber tip. Several series of measurements were taken in this way, but the most relevant and careful measurements, which are shown in Figure 4.5, were taken at distances from 0 to 5mm vertically from the fiber tip in 1 mm increments. Taking such measurements requires some image processing, because the range of intensities present on the screen exceeds the dynamic range of the digital camera. An image with a long exposure time becomes saturated, while short exposure times do not detect the lower intensities in the tails of the distribution. To overcome this limitation, and acquire an accurate distribution over the full range of intensities that can be observed, multiple exposures are taken at every position. Using the known exposure times, intensities from each image are divided by the exposure time, to normalize them, so they can be directly compared. It was found that the most accurate normalized intensity values were consistently the highest ones, as shown in Figure 4.6. Using MATLAB to choose, at each pixel, the largest normalized intensity, these images are merged to form a single distribution. Figure 4.7 shows 3 such distributions as surface plots for a series of distances from the fiber tip. The distribution most relevant for the

TEM (2mm distance) is also shown in the inset as a contour plot. In the y direction, the FWHM is 1.06mm, and the peak is Gaussian while in the x direction, the FWHM is 2.45mm, and the peak shape is more complex. The maximum intensity is 1456mW/cm^2.

In-Situ Spatial Characterization of Light

Precise alignment of the light on the TEM sample is essential. Immediately after the fiber manipulator has been mounted onto the TEM column, a process which requires the column vacuum to be broken, the initial alignment may be observed directly, by removing the objective aperture blade, and viewing the fiber tip through the objective aperture port. After this rough alignment has been completed, a specially constructed photodiode detector is inserted into the TEM via the specimen airlock. This small photodiode has been built into a TEM sample holder rod, as shown in Figure 4.8, and can be precisely positioned at the sample position between the upper and lower objective lens pole pieces. The details of this sample holder photodiode detector are given in Appendix D. This allows the location and intensity of the light beam to be directly determined. The size of the photodiode is quite large at about 1mm^2 considering that the light distribution on the sample is only about 1mm wide and 2mm long so that at any given detector position, a large area of the light distribution is sampled. However, despite the large size of the detector, its position can be varied quite precisely, using the sample stage of the microscope. It is thus straightforward to find the point of highest intensity in the light distribution, and then move the fiber tip accordingly to center the maximum intensity on the electron optical axis. Before the success of any alignment can be evaluated, it is important to know just how precisely the

fiber must be aligned to achieve an acceptably high light intensity at the electron beam position. Measurements of the distribution obtained using optical microscopy given in Figure 4.9 as a contour plot yield a condition for alignment of the fiber with respect to the optic axis of the microscope. To maintain an intensity level at the optic axis of at least 90% of the maximum, the distribution must be within 0.4mm of centered in the X direction, and within 0.2mm of centered in the Y direction.

The *in-situ* technique for light characterization grows out of this photodiode sample holder alignment procedure. The position of the photodetector is systematically varied using the sample stage of the microscope. This can produce either simple line profiles, as shown in Figure 4.10, or a full 2D distribution, as given in Figure 4.11. From Figure 4.10 it is clear that the intensity falling on the detector has a well defined maximum when it is translated along the x, y and z directions. Measurements show that the maximum is significantly broader than the maximum seen in the distribution characterized ex-situ, because the detector area is large, thus smoothing the measured intensity distribution. From the angular dependence, it can be seen that the measured intensity increases as the photodiode is tilted around the sample rod axis so that it more closely aligns to face the light beam direction, as one would expect.

Correlating the precise distributions produced using the optical microscope, with the *in situ* measurements from the photodiode inside the microscope, after the fiber has been aligned, it is possible to calculate the intensity that is incident on the TEM sample, with good accuracy, and reasonable spatial resolution. This is

essential for interpreting results obtained using this illumination technique. The intensity that is achieved on the TEM sample on the optic axis is 1460 mW/cm^2. Scaling the distribution obtained using the optical microscope to this maximum intensity value, it is possible to integrate the distribution to obtain the total power in the beam emitted by the fiber inside the microscope. The total power is 45.63 mW which is about 6% of the nominal power emitted by the light source as shown in Figure 4.12

Light Power, Losses

While 6% may seem to be a very small number, most of the losses have been well accounted for, and are not easily reduced; they arise from several sources. The first and most serious source of loss is that approximately 65% of the light from the light source does not come directly from the point source, and cannot be focused onto the fiber, as shown in Figure 4.13. Because the inside surfaces of the light source housing are highly reflective, much of the light that exits the aperture of the source has been reflected off the walls, and does not come directly from the point source. This is a defect of the lamp design, and the specifications of the light source should more clearly indicate this issue, by specifying the focusable power of the light as well as the total power exiting the aperture of the source. The only way to increase the percentage of the light emitted by the source that can be focused by the parabolic mirrors, would be to install a concave spherical mirror within the light housing itself, that would focus light emitted from the source, directly back to its point of origin, as shown in Figure 4.14. This could have adverse effects on the source however, so it has not been attempted. Another 22% of the light is lost due to known optical imperfections; these cannot

be totally eliminated, because no optical material is perfect, and some absorption always occurs as light goes through an optical system. A spectrum showing the total expected optical losses of the system as a function of wavelength is given in Figure 4.2. Finally, 7% of the light has not been accounted for precisely, and this loss may be due to optics that do not meet the manufacturers' specifications, or to slight misalignments. Despite these significant losses, substantial intensity still reaches the TEM sample, and in the visible range the intensity is 10 times that of the AM 1.5 solar spectrum, as seen in Figure 3.3.

Characterizing Microscope Performance

Microscope performance has also been evaluated. Initial experiments conducted while illuminating the TEM sample have shown that the electron optical performance of the microscope is not degraded noticeably by the addition of the fiber illumination system. Figure 4.15 shows an example of a particle of TiO2 which has been observed over the course of several days in the presence of water vapor and at 150°C. At the beginning of the experiment, the light source was turned off, as shown in the image on the left. The right image shows the same particle being illuminated by the light source. In both images lattice fringes of 2.5nm can be seen in the FFT. In a more demanding test, given in Figure 4.16, the information limit of the microscope is shown to be unchanged by the addition of the light source. Both diffractograms shown are calculated from images that were taken while the fiber is in its working position, and clearly show Au {220} lattice fringes out to 0.144nm, near the quoted value of the information limit of the Tecnai F20 (0.14nm) This demonstrates that the microscope's resolution is not degraded by charging of the fiber tip, or magnetic interference from the fiber or

guide rods. The image on the right is also taken with the light source turned on, indicating that any vibrations or EM interference produced by the light source are also not degrading microscope performance.

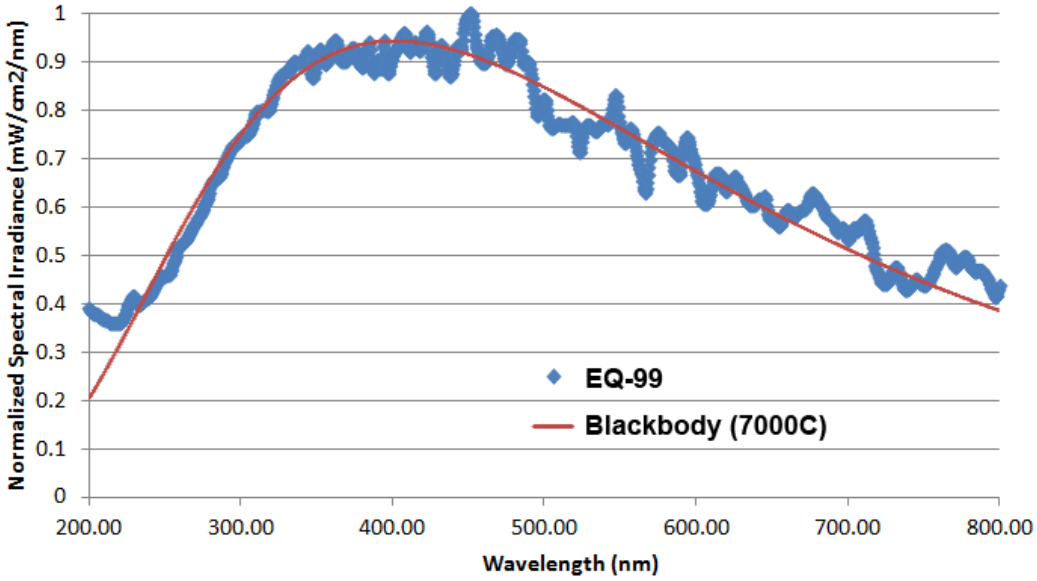

Figure 4.1 Blackbody fit to EQ-99 Spectrum

The light source spectrum before optics is fit here by a blackbody curve. The fit gives a temperature of about 7000°C. This is only slightly hotter than the sun.

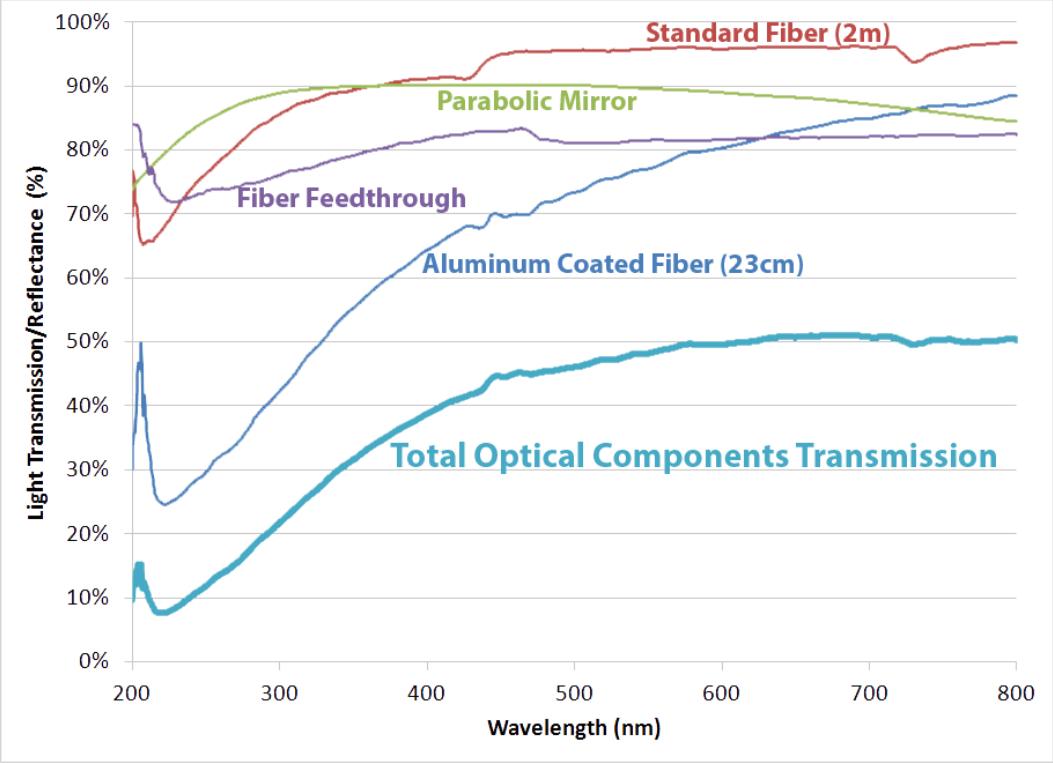

Figure 4.2 Optical Components Transmission Spectra

The transmission (or reflectance in the case of the mirrors) of all the optical components in the system. The total composite spectrum shows the transmission of light through the entire optical system, including mirrors, fibers, and the fiber feedthrough, and demonstrates why the losses from the optical components are so large in Figure 4.12.

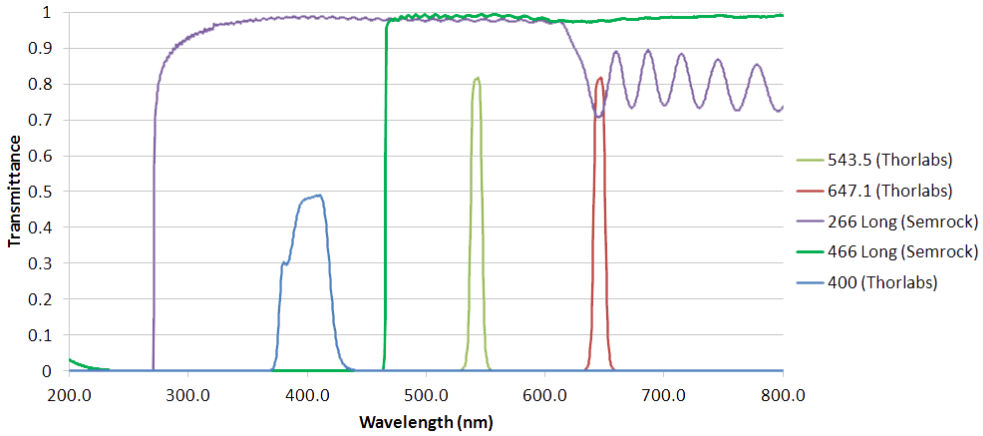

Figure 4.3 Filters Spectra

Transmittance of the 5 filters currently purchased for this research. Of these 3 are bandpass filters from Thorlabs, and 2 are Longpass filters from Semrock.

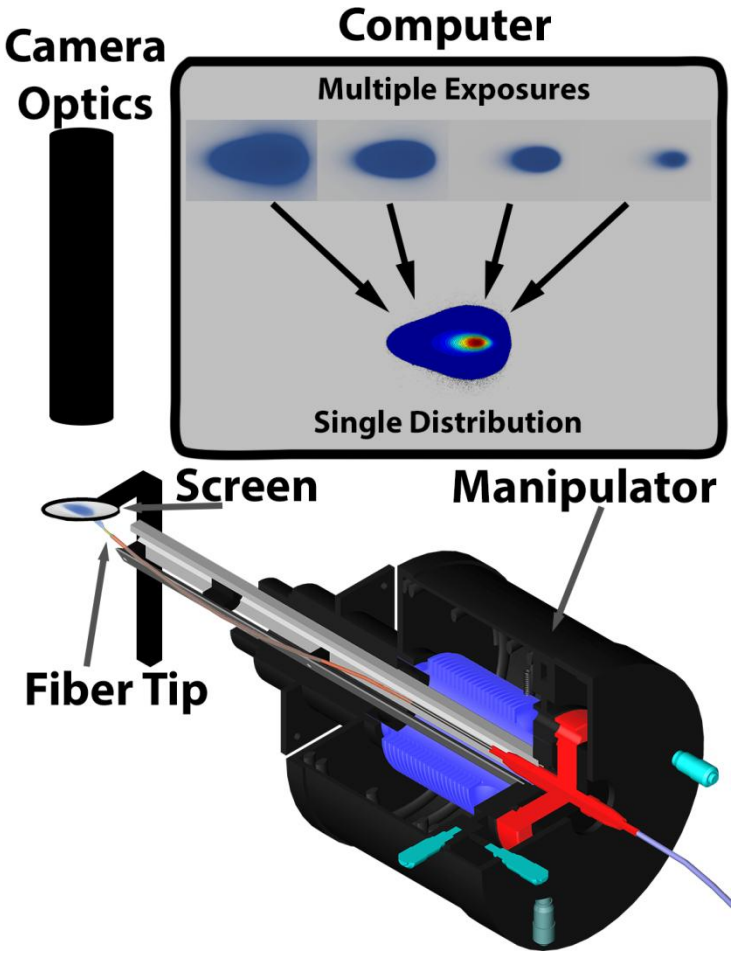

Figure 4.4 Ex Situ Characterization Setup

A schematic showing the experimental setup used to measure the light intensity distribution outside the TEM. An optical microscope camera is used to take images of the light distribution as seen on a small moveable screen which is kept in the horizontal plane. Since the dynamic range of the camera is not large enough to image the entire distribution, at each position of the fiber relative to the screen, multiple exposures are imaged. These are then combined to generate a single intensity distribution.

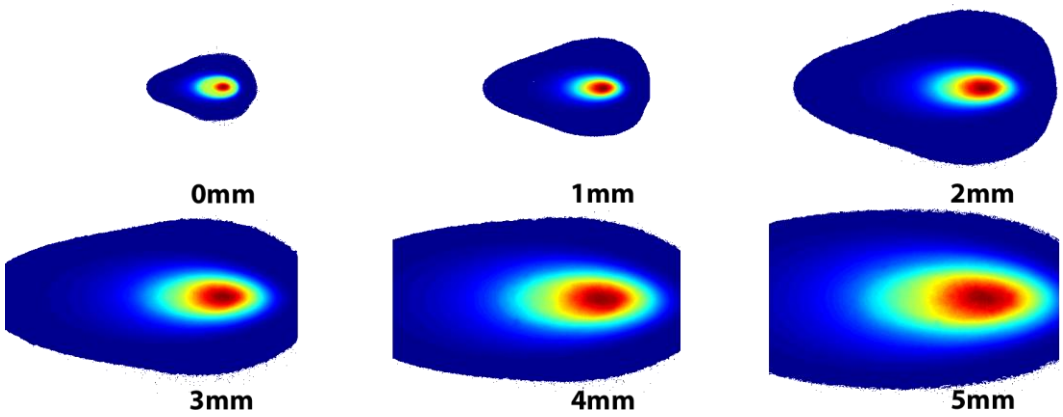

Figure 4.5 Measured Intensity Distributions.

The intensity distributions measured using the optical microscope for a series of distances from the fiber tip are given here. The distances given are the vertical distance from the top of the fiber tip to the bottom of the screen. Each distribution is normalized to the peak intensity for clarity.

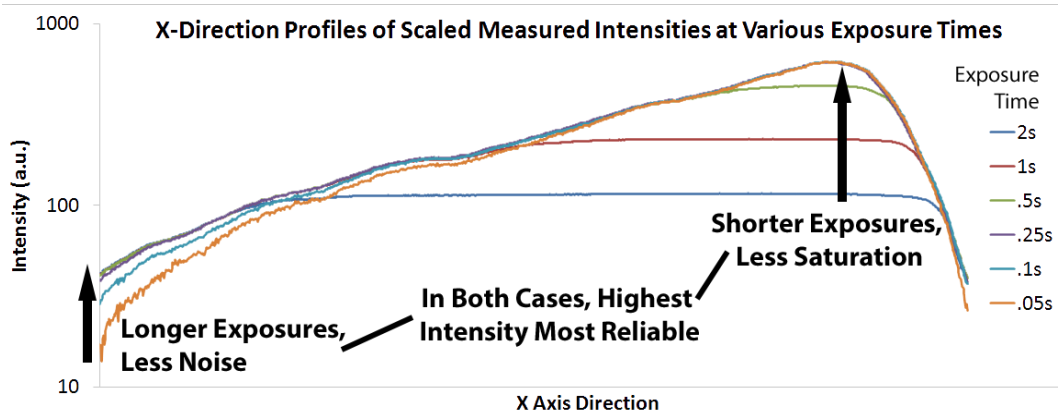

Figure 4.6 Exposure Times Comparison

Profiles in the X direction of the scaled intensities measured using the optical microscope camera at various exposure times. Because the dynamic range of the camera is too small to accurately measure all intensities simultaneously, several exposures are taken. These are then scaled according to their exposure times. At all points in the distribution it is found that the highest scaled intensity is most reliable, and so it is simple to combine the various exposures by choosing the maximum at every point in the distribution.

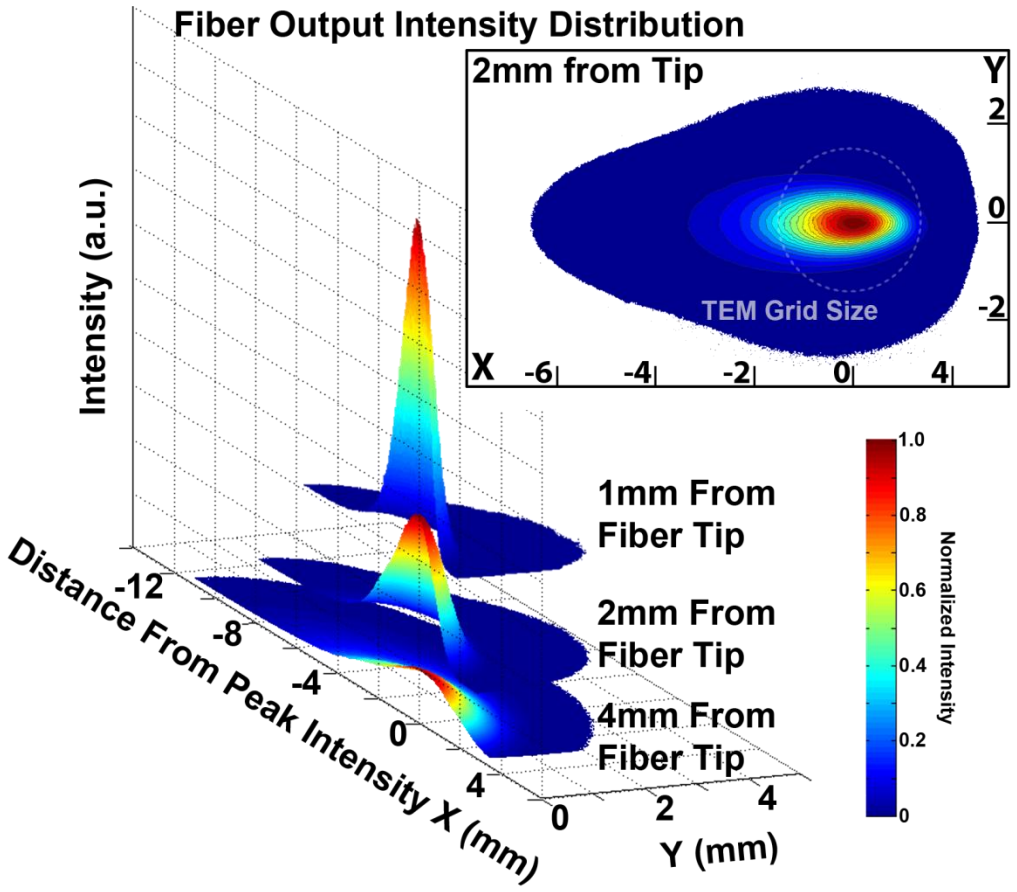

Figure 4.7 Measured Distribution Surface Plots

Surface plots of the measured distribution at 3 different distances from the fiber tip are shown here. These are identically scaled in the intensity axis and offset, so the the spreading of the beam as distance increases can be clearly seen, though the colors are normalized in each plot. The inset shows a filled contour plot of the 2mm distance with contours at every 5% of the maximum intensity. 2mm is approximately the actual distance inside the TEM. The inset also provides a sense of scale by including a dashed circle the size of a standard 3mm TEM sample grid.

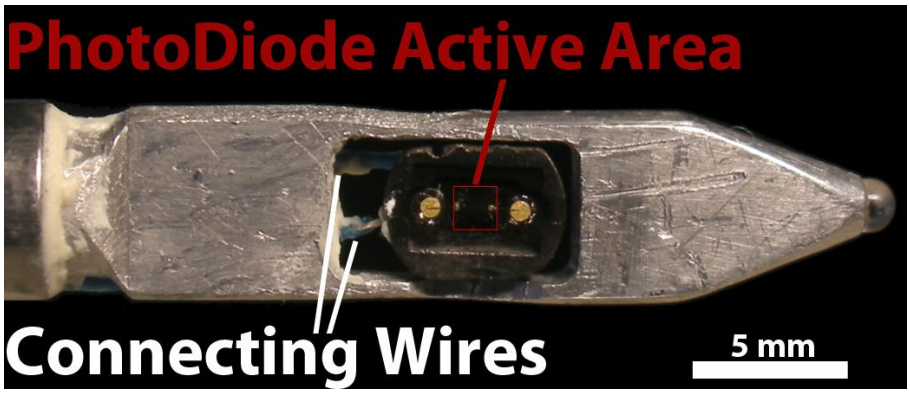

Figure 4.8 Photodiode Holder

This photo shows the custom built TEM holder, which houses a photodiode. This holder allows the intensity at the TEM sample position to be measured *in situ* in the microscope. The active area of the photodiode is about $1mm^2$, the size of the small red square.

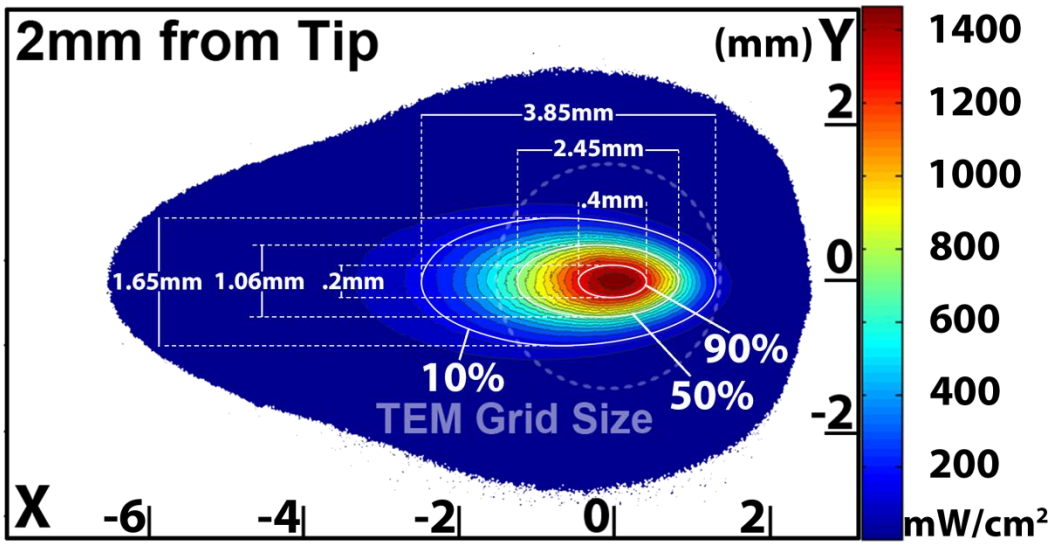

Figure 4.9 Intensity Distribution with Measurements

The same distribution as in the inset in Figure 4.7 is shown here. Three black contours are given and labeled at 10%, 50%, and 90% of the maximum intensity. The widths of these contours in both the X and Y directions are also labeled. The axes scale is mm.

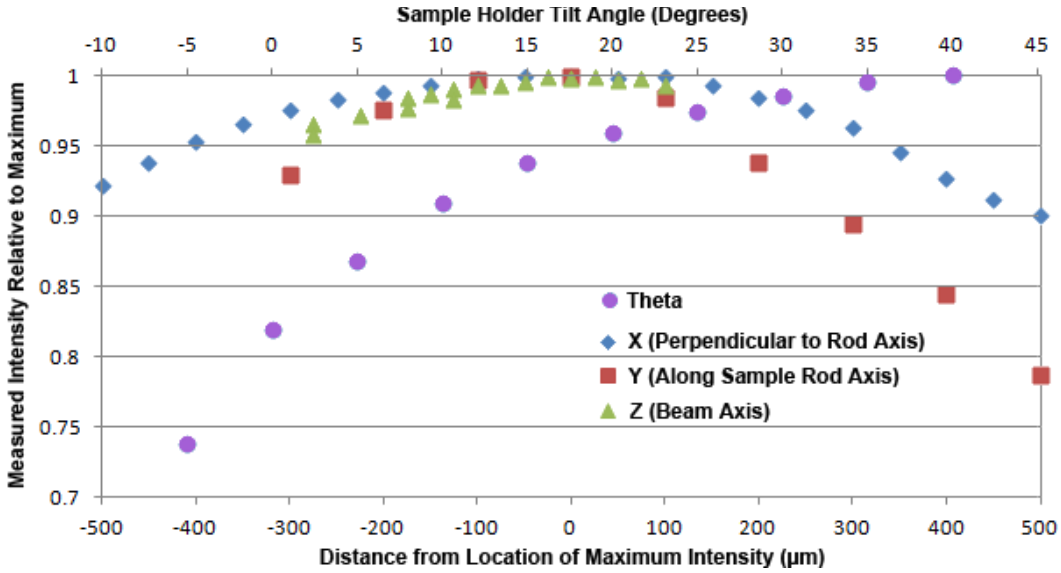

Figure 4.10 *In Situ* Intensity Measurements

The results of using the sample holder mounted photodiode to measure the intensity as a function of position inside the microscope. The lower axis gives the distance from the location of maximum intensity along all three Cartesian directions, (defined in Figure 3.9) which can be precisely varied using the translation stage of the microscope. The upper axis shows the rotation around the sample holder axis. All measurement series are normalized relative to their maximum value.

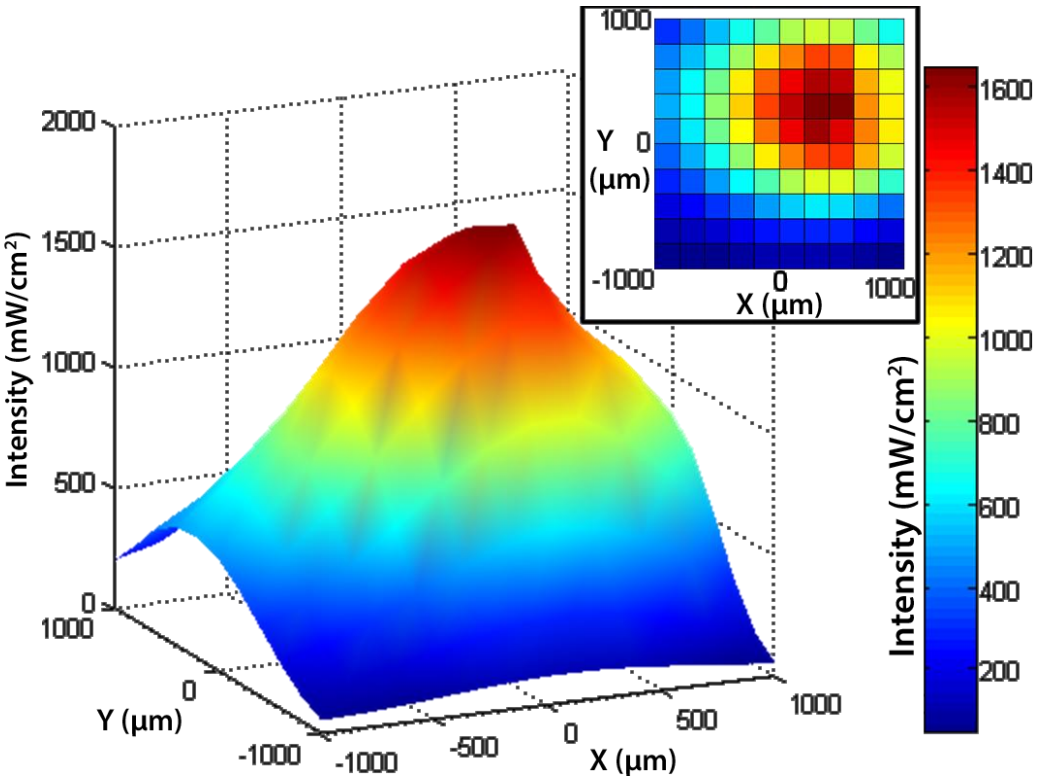

Figure 0.1 *In Situ* Light Distribution Characterization

The distribution of the light was measured *in situ* using the photodiode holder which is moved systematically by the microscope stage. The distribution is shown here as an interpolated surface plot as well as the original data from the top in the insert. Only a 2mm2 area can be measured because of the limits of the microscope stage.

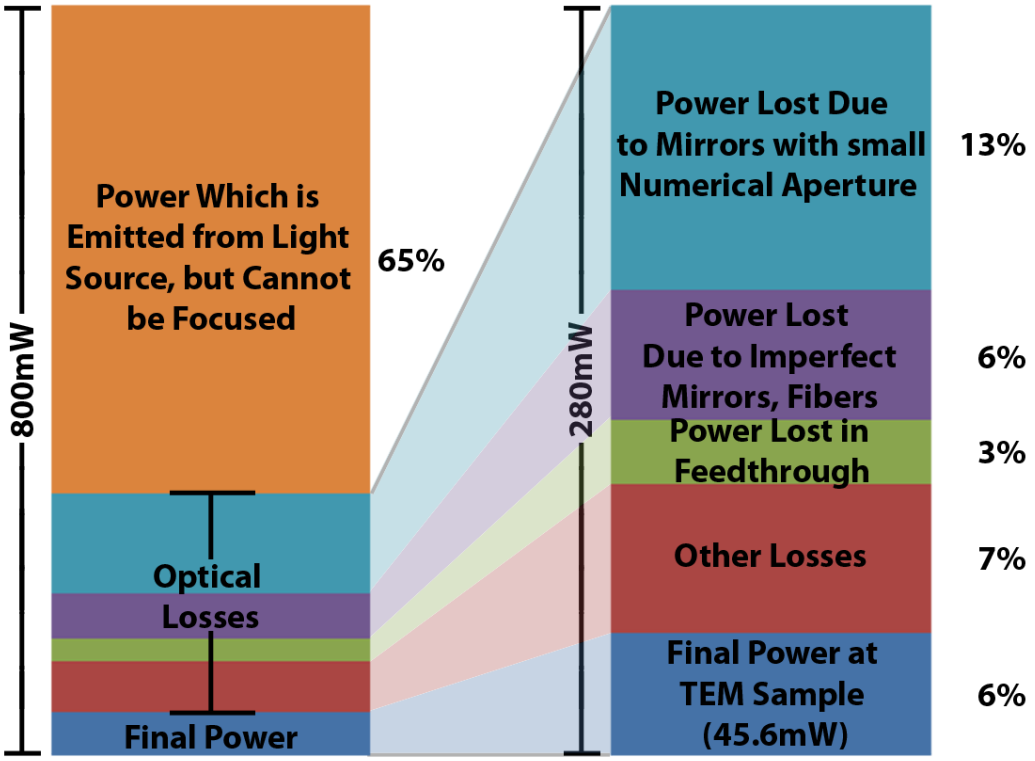

Figure 4.12 Power Losses in the Optical System

The left bar shows the various amounts with resepect to the full power emitted from the light source aperture (800mW). However, since much of this light comes from reflections within the bulb housing, not directly from the point source, this light cannot all be focussed back to a small point. In fact, only 280mWof the light comes from the point source, and the losses associated with this light are shown in the right side bar. While the final power reaching the TEM sample is only 45.6mW, this still yields an intensity of about 1460mW/cm^2 at the electron beam location.

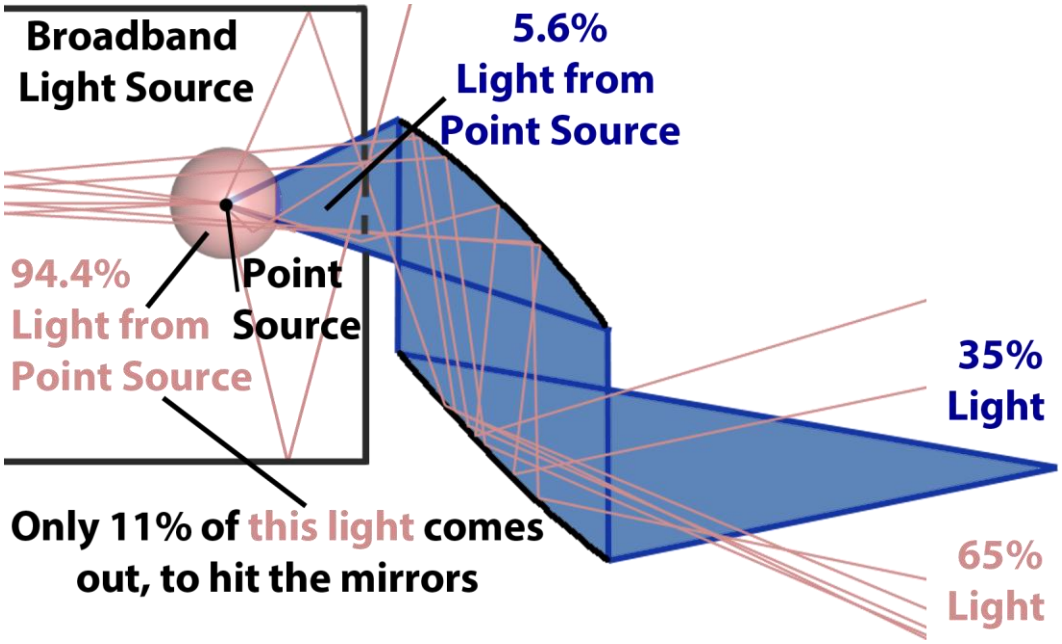

Figure 4.13 Focusable Light

This schematic diagram shows how a significant portion of the light exiting the source aperture does not come directly from the point source, but rather from reflections within the housing. Since only 5.6% of the spherically symmetric emmission exits directly through the aperture, most of the light that comes out has been reflected at least once already. This light cannot be focused back to the same point with the mirrors, and thus, only 35% of the light exiting the source can be focused.

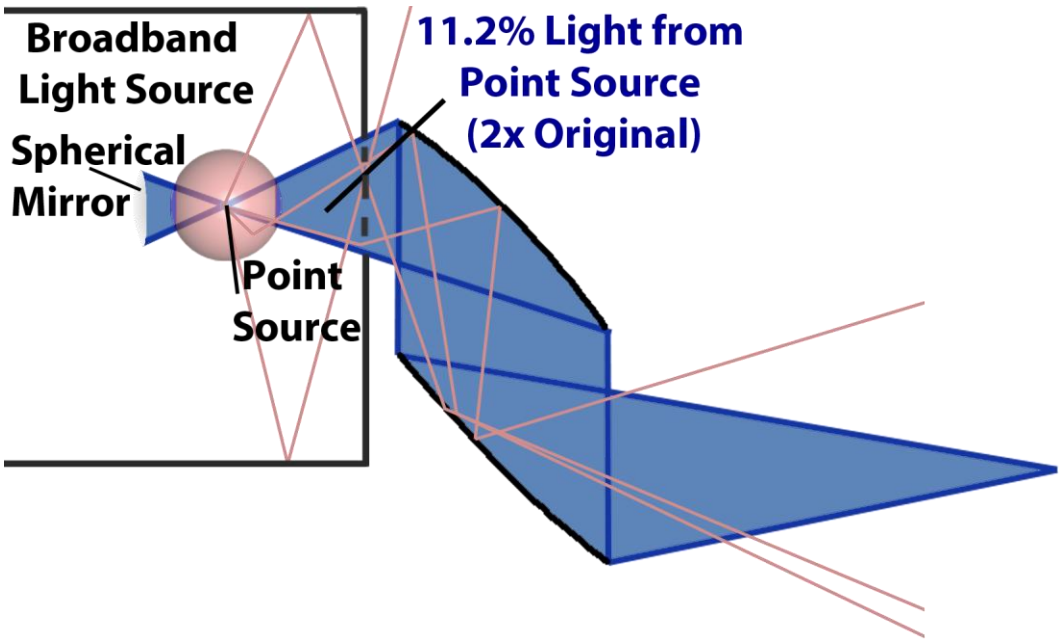

Figure 4.14 Future Proposed Modification

Adding a spherical mirror behind the bulb in the light source housing might theoretically double the amount of focusable light exiting the aperture of the source. This has not been attempted, and should be done in consultation with the company who designed the light, since the housing is not meant to be disassembled by the user.

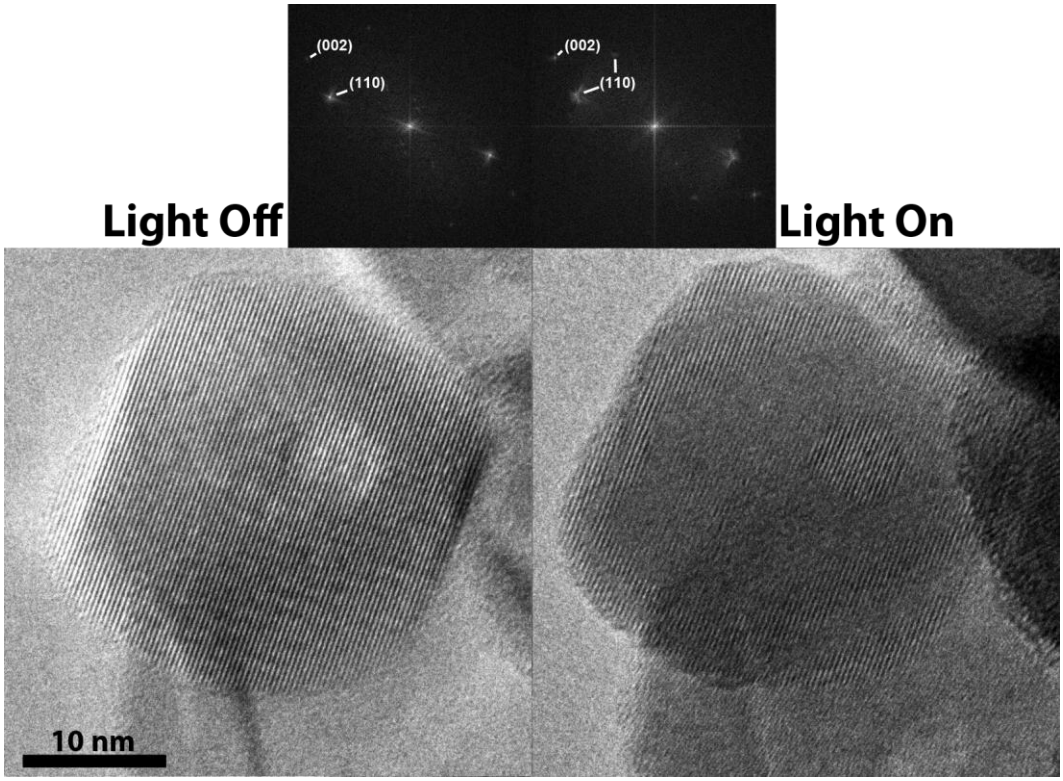

Figure 4.15 Initial Images

Two images of one particle of anatase TiO_2. The left image was taken with the light off, while the right image is taken with the light on, as well as with 67 Pa (.5 torr) of water vapor and heated to 150°C. The diffractograms of both images show faint lattice fringes at about 2.5nm, corresponding to the (002) planes, demonstrating that the lattice can still be observed while heating and illuminating the sample in a gaseous environment.

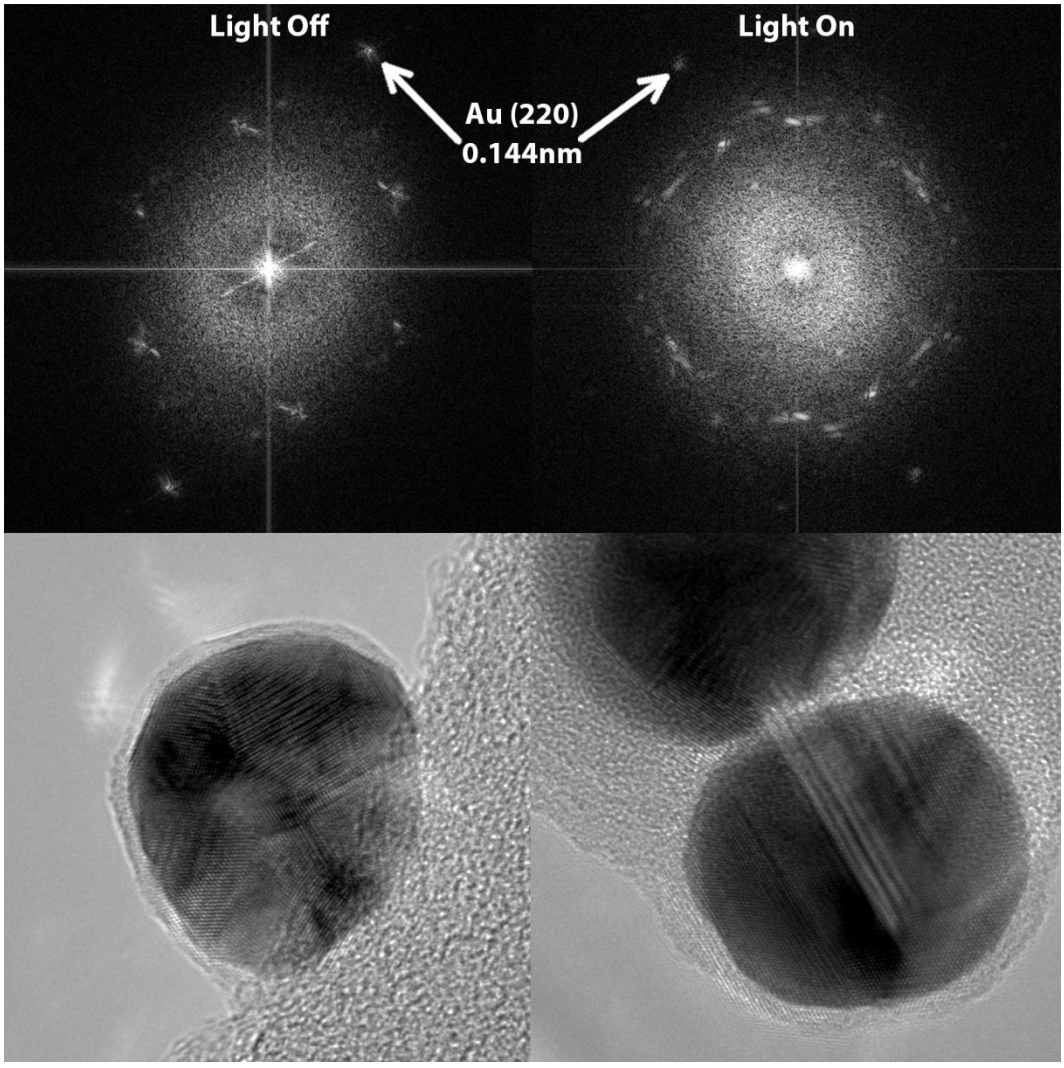

Figure 4.16 Resolution Check

Images (bottom) and diffractograms generated by Digital Micrograph (top) of two different gold particles are shown. The diffractogram on the left shows information being transferred up to 0.144nm when the light is off, while the diffractogram on the right shows a similar information limit while the light is turned on.

CONCLUSIONS

Summary of Current Accomplishments

In summary, a light illumination system has been designed and built which fulfils the functionality that was desired, and does not degrade the performance of the microscope. An optics system was put together which takes the light produced by a broadband bright source, and focuses it into an optical fiber after optionally passing through a filter to modify the spectral range. The light passes through a feedthrough into the high vacuum of the microscope, into a specially designed fiber. This fiber is compatible with the high vacuum, as well as being robust in reactive gasses, and heating, and is non-magnetic and conductive. It is also cut at the tip, so that the maximum intensity ($1460 mW/cm^2$) of the light distribution is directed onto the sample at the electron optic axis position on the TEM sample. This fiber can be precisely positioned to achieve this alignment with the TEM sample, yet may be retracted when not in use. The light distribution within the microscope has been precisely characterized outside the microscope, and has also been observed *in situ* using the same photodiode that is used for the alignment procedure, which is installed in a custom TEM holder.

Future Work

The system designed for the Tecnai is complete, and functional. It is currently being used in ongoing experiments to study the effects of UV light on a titania photocatalyst. However, some future modifications may be desirable. In the light source itself, it would be beneficial if a spherical mirror could be placed inside the

housing, behind the bulb, to reflect light that is emitted in the opposite direction from the source aperture, back through the point source and out to the rest of the optical system. In the optical system, it might be beneficial to purchase tunable filters, which pass a different wavelength range based on the angle that the light passes through the filter. This would allow a small set of filters to yield any wavelength in the visible or UV range. However, this would require that the location of the filters be changed, since the light beam must be parallel, not convergent as it passes through such a filter. The manipulator would have increased performance, if the springs that are normal to the fiber direction were stiffer. This is a relatively simple fix, but has not been completed, since the manipulator still functions well enough to properly align the fiber. It would also be nice, though not necessary to fix the MATLAB code so that the measured and calculated distributions match more closely. This has been attempted several times, but the solution was never found. Finally, while the in-situ and ex-situ light distribution measurements are in qualitative agreement, more work is needed to quantitatively compare the two. Such a correlation would allow the precise distance of the fiber from the TEM sample to be determined, as it is only approximately known at the present.

In addition to these small changes, it should be noted that as mentioned briefly in the context section of this document, a similar system has been planned for a microscope that will be delivered to Arizona State in the next year. This microscope from NION will be Cs corrected, and will also have a monochromator, which will allow unprecedented EELS resolution. This improved

spatial and energy resolution should allow the study, of electronic changes in materials produced by the interaction of the material with the light. Unlike any other currently available technique, the observed changes will be spatially resolved down to the nanoscale. This may provide insights into the fundamental processes involved in nanoscale materials which respond to illumination. Modifying the NION microscope will require a new design for the fiber and supports within the microscope, since the dimensions are different, and more obstacles are present around the sample area. The optical system can be identical however, and depending on the amount of use the light source sees, the same source may be used for both microscopes, as it can be taken apart, transported, set up, and realigned in less than an hour.

There are of course, many experiments that can be imagined as future work on the microscope equipped with this capability to illuminate the sample. While nanoparticles of anatase TiO2 are currently being studied in the ETEM using the light illumination, other titania morphologies such as nanotubes and nanorods could also be studied in the future. Silver halide nanoparticles used in photochromic glass have been studied in the past using TEM (Rincon, Marquez, and Rivera 1991; OLESHKO et al. 1995) as the mechanism for the reversible reaction induced by UV light is not entirely understood. This is another good candidate system for study using this new capability, since a reversible structural change in the material is driven by UV irradiation. Also interesting is the behavior of silver nanoparticles under UV irradiation. Silver particles are known to coalesce and grow under UV irradiation (Badger and Hummel 1945; Callegari,

Tonti, and Chergui 2003) and this behavior might be able to be studied in real time in the TEM using the light. Of course, titania is not the only nanostructured photocatalyst being worked on today, and other systems, including Tantalates (Kudo and Miseki 2009; Kato, Asakura, and Kudo 2003), strontium titanates (Wagner and Somorjai 1980), and GaN:ZnO based photocatalysts (Kazuhiko Maeda et al. 2010) could also be studied *in situ* using this illumination system. Many opportunities now exist to pursue research using this new capability, and so much more hard work will be required.

REFERENCES

Badger, A., and F. Hummel. 1945. “Effect of Ultraviolet Light on Glass Containing Silver.” *Physical Review* 68 (9-10) (November): 231–231. doi:10.1103/PhysRev.68.231.

Bell, A.T., B.C. Gates, D. Ray, and M.R. Thompson. 2008. *Basic Research Needs: Catalysis for Energy*. Pacific Northwest National Laboratory (PNNL), Richland, WA (US).

Callegari, A., D. Tonti, and M. Chergui. 2003. “Photochemically Grown Silver Nanoparticles with Wavelength-Controlled Size and Shape.” *Nano Letters* 3 (11) (November): 1565–1568. doi:10.1021/nl034757a.

Cavalca, F., AB Laursen, B.E. Kardynal, RE Dunin-Borkowski, S. Dahl, JB Wagner, and T.W. Hansen. 2012. “In Situ Transmission Electron Microscopy of Light-induced Photocatalytic Reactions.” *Nanotechnology* 23: 075705.

Chenna, Santhosh. 2011. “In-situ Environmental TEM Studies For Developing Structure-Activity Relationship in Supported Metal Catalyst”. United States -- Arizona: Arizona State University. http://login.ezproxy1.lib.asu.edu/login?url=http://search.proquest.com/docview/907550945?accountid=4485.

Chenna, Santhosh, Ritubarna Banerjee, and Peter A. Crozier. 2011. “Atomic-Scale Observation of the Ni Activation Process for Partial Oxidation of Methane Using In Situ Environmental TEM.” *ChemCatChem* 3 (6) (June 14): 1051–1059. doi:10.1002/cctc.201000238.

Chenna, Santhosh, and Peter A. Crozier. 2012. “In Situ Environmental Transmission Electron Microscopy to Determine Transformation Pathways in Supported Ni Nanoparticles.” *Micron* (May). doi:10.1016/j.micron.2012.04.007. http://linkinghub.elsevier.com/retrieve/pii/S0968432812001308.

Colliex, C. 2011. “From Electron Energy-loss Spectroscopy to Multi-dimensional and Multi-signal Electron Microscopy.” *Journal of Electron Microscopy* 60 (supplement 1) (August 15): S161–S171. doi:10.1093/jmicro/dfr028.

Cox, P. M, R. A Betts, C. D Jones, S. A Spall, I. J Totterdell, and others. 2000. “Acceleration of Global Warming Due to Carbon-cycle Feedbacks in a Coupled Climate Model.” *Nature* 408 (6809): 184–187.

Crozier, Peter A., and Santhosh Chenna. 2011. “In Situ Analysis of Gas Composition by Electron Energy-loss Spectroscopy for Environmental

Transmission Electron Microscopy." *Ultramicroscopy* 111 (3) (February): 177–185. doi:10.1016/j.ultramic.2010.11.005.

Crozier, Peter A., Ruigang Wang, and Renu Sharma. 2008. "In Situ Environmental TEM Studies of Dynamic Changes in Cerium-based Oxides Nanoparticles During Redox Processes." *Ultramicroscopy* 108 (11) (October): 1432–1440. doi:10.1016/j.ultramic.2008.05.015.

Grätzel, Michael. 2009. "Recent Advances in Sensitized Mesoscopic Solar Cells." *Accounts of Chemical Research* 42 (11) (November 17): 1788–1798. doi:10.1021/ar900141y.

Hansen, P. L. 2002. "Atom-Resolved Imaging of Dynamic Shape Changes in Supported Copper Nanocrystals." *Science* 295 (5562) (March 15): 2053–2055. doi:10.1126/science.1069325.

Kato, H., K. Asakura, and A. Kudo. 2003. "Highly Efficient Water Splitting into H2 and O2 over Lanthanum-doped NaTaO3 Photocatalysts with High Crystallinity and Surface Nanostructure." *Journal of the American Chemical Society* 125 (10): 3082–3089.

Krivanek, O. L., J. P. Ursin, N. J. Bacon, G. J. Corbin, N. Dellby, P. Hrncirik, M. F. Murfitt, C. S. Own, and Z. S. Szilagyi. 2009. "High-energy-resolution Monochromator for Aberration-corrected Scanning Transmission Electron Microscopy/electron Energy-loss Spectroscopy." *Philosophical Transactions of the Royal Society A: Mathematical, Physical and Engineering Sciences* 367 (1903) (August 17): 3683–3697. doi:10.1098/rsta.2009.0087.

Kudo, Akihiko, and Yugo Miseki. 2009. "Heterogeneous Photocatalyst Materials for Water Splitting." *Chemical Society Reviews* 38 (1): 253. doi:10.1039/b800489g.

LaGrange, T., M. R. Armstrong, K. Boyden, C. G. Brown, G. H. Campbell, J. D. Colvin, W. J. DeHope, et al. 2006. "Single-shot Dynamic Transmission Electron Microscopy." *Applied Physics Letters* 89 (4): 044105. doi:10.1063/1.2236263.

LaGrange, Thomas, Geoffrey H. Campbell, B.W. Reed, Mitra Taheri, J. Bradley Pesavento, Judy S. Kim, and Nigel D. Browning. 2008. "Nanosecond Time-resolved Investigations Using the in Situ of Dynamic Transmission Electron Microscope (DTEM)." *Ultramicroscopy* 108 (11) (October): 1441–1449. doi:10.1016/j.ultramic.2008.03.013.

Leyva Porras, Cesar. 2010. “Photoreduction of Carbon Dioxide with Hydrogen on Well Dispersed Copper Particles on Titanium Dioxide Photocatalyst”. United States -- Arizona: Arizona State University.

Li, P., J. Liu, N. Nag, and P. A. Crozier. 2004. “In-Situ Environmental TEM Study on the Synthesis of Ni/TiO2 Catalysts Under Different Gas Environments.” *Microscopy and Microanalysis* 10 (S02) (August 1). doi:10.1017/S1431927604885301. http://www.journals.cambridge.org/abstract_S1431927604885301.

Maeda, K. 2011. “Photocatalytic Water Splitting Using Semiconductor Particles: History and Recent Developments.” *Journal of Photochemistry and Photobiology C: Photochemistry Reviews*.

Maeda, Kazuhiko, Anke Xiong, Taizo Yoshinaga, Takahiro Ikeda, Naoyuki Sakamoto, Takashi Hisatomi, Masaki Takashima, et al. 2010. “Photocatalytic Overall Water Splitting Promoted by Two Different Cocatalysts for Hydrogen and Oxygen Evolution Under Visible Light.” *Angewandte Chemie* 122 (24) (June 1): 4190–4193. doi:10.1002/ange.201001259.

Murakami, Y., N. Kawamoto, D. Shindo, I. Ishikawa, S. Deguchi, K. Yamazaki, M. Inoue, Y. Kondo, and K. Suganuma. 2006. “Simultaneous Measurements of Conductivity and Magnetism by Using Microprobes and Electron Holography.” *Applied Physics Letters* 88 (22): 223103. doi:10.1063/1.2208384.

OLESHKO, V., R. GIJBELS, W. JACOB, and M. ALFIMOV. 1995. “Characterization Of Complex Silver-Halide Photographic Systems By Means Of Analytical Electron-Microscopy.” *Microbeam Analysis* 4 (1) (February): 1–29.

Owen, N. A, O. R Inderwildi, and D. A King. 2010. “The Status of Conventional World Oil reserves—Hype or Cause for Concern?” *Energy Policy* 38 (8): 4743–4749.

Rincon, J. M., H. Marquez, and E. Rivera. 1991. “Electron Microscopy and EDX-microanalysis of Photochromic Silver Halide Glasses of the Composition Systems Al2O3-B2O3-SiO2 and Na2O-CaO-SiO2.” *Journal of Materials Science* 26 (5): 1192–1198. doi:10.1007/BF00544454.

Santra, S, and P Crozier. 2011. “In-situ Environmental TEM Study of Phase and Morphological Changes of TiO2 Nanotubes Under Different Heat Treatments.” *Microscopy and Microanalysis* 17 (S2) (October 7): 1600–1601. doi:10.1017/S1431927611008877.

Sharma, Vaneet. 2011. “Synthesis and In Situ Environmental Transmission Electron Microscopy Investigations of Ceria-Based Oxides for Solid Oxide Fuel Cell Anodes”. United States -- Arizona: Arizona State University. http://login.ezproxy1.lib.asu.edu/login?url=http://search.proquest.com/docview/913537776?accountid=4485.

Sharma, Vaneet, Peter A. Crozier, Renu Sharma, and James B. Adams. 2012. “Direct Observation of Hydrogen Spillover in Ni-loaded Pr-doped Ceria.” *Catalysis Today* 180 (1) (January): 2–8. doi:10.1016/j.cattod.2011.09.009.

Shindo, D., K. Takahashi, Y. Murakami, K. Yamazaki, S. Deguchi, H. Suga, and Y. Kondo. 2009. “Development of a Multifunctional TEM Specimen Holder Equipped with a Piezodriving Probe and a Laser Irradiation Port.” *Journal of Electron Microscopy* 58 (4): 245–249.

Taheri, Mitra L., Thomas Lagrange, Bryan W. Reed, Michael R. Armstrong, Geoffrey H. Campbell, William J. DeHope, Judy S. Kim, Wayne E. King, Daniel J. Masiel, and Nigel D. Browning. 2009. “Laser-based in Situ Techniques: Novel Methods for Generating Extreme Conditions in TEM Samples.” *Microscopy Research and Technique* 72 (3) (March): 122–130. doi:10.1002/jemt.20664.

Topsoe, H. 2003. “Developments in Operando Studies and in Situ Characterization of Heterogeneous Catalysts.” *Journal of Catalysis* 216 (1-2): 155–164.

Wagner, F. T., and G. A. Somorjai. 1980. “Photocatalytic and Photoelectrochemical Hydrogen Production on Strontium Titanate Single Crystals.” *Journal of the American Chemical Society* 102 (17) (August): 5494–5502. doi:10.1021/ja00537a013.

Wang, Ruigang, Peter A. Crozier, and Renu Sharma. 2009. “Structural Transformation in Ceria Nanoparticles During Redox Processes.” *The Journal of Physical Chemistry C* 113 (14) (April 9): 5700–5704. doi:10.1021/jp8107232.

Woyte, A., V.V. Thong, R. Belmans, and J. Nijs. 2006. “Voltage Fluctuations on Distribution Level Introduced by Photovoltaic Systems.” *IEEE Transactions on Energy Conversion* 21 (1) (March): 202–209. doi:10.1109/TEC.2005.845454.

Yoshida, K., T. Nozaki, T. Hirayama, and N. Tanaka. 2007. “In Situ High-resolution Transmission Electron Microscopy of Photocatalytic Reactions by Excited Electrons in Ionic Liquid.” *Journal of Electron Microscopy* 56 (5): 177.

Yoshida, Kenta, Takahiro Nanbara, Jun Yamasaki, and Nobuo Tanaka. 2006. “Oxygen Release and Structural Changes in TiO[sub 2] Films During

Photocatalytic Oxidation." *Journal of Applied Physics* 99 (8): 084908. doi:10.1063/1.2190721.

Yoshida, Kenta, Jun Yamasaki, and Nobuo Tanaka. 2004a. "In Situ High-resolution Transmission Electron Microscopy Observation of Photodecomposition Process of Poly-hydrocarbons on Catalytic TiO[sub 2] Films." *Applied Physics Letters* 84 (14): 2542. doi:10.1063/1.1689747.

———. 2004b. "A Trial for in Situ Quantitative TEM–EELS Measurement Related to the Photoreaction Process of TiO2 Films." *Nanotechnology* 15 (6) (June): S349–S354. doi:10.1088/0957-4484/15/6/006.

Zalba, B., J. M Marín, L. F Cabeza, and H. Mehling. 2003. "Review on Thermal Energy Storage with Phase Change: Materials, Heat Transfer Analysis and Applications." *Applied Thermal Engineering* 23 (3): 251–283.

APPENDIX A

LIGHT SOURCE-MIRRORS MISALIGNMENT

The light source produced by Energetiq was sold complete with the series of two parabolic mirrors which were designed to focus the light from the source back to a small spot, to be coupled into an optical fiber. The initial results of this setup were quite disappointing, and the intensity passing into the fiber was less than 4%. An extensive search for the causes of this very low coupling efficiency revealed many factors, some of which were discussed in the text as losses that cannot be avoided. However, one of the initial loss mechanisms was found to be improper alignment of the optics by the engineers from Energetiq. The mirrors used in the design are small, circular sections of paraboloids. This means that they focus all the light coming parallel to their axis of symmetry to their focal point. Thus, if the focal point of the first mirror is the light source, and that of the second mirror is an optical fiber, and the mirrors are the same size and aligned to each other, the light will be correctly focused onto the fiber. This is shown in the figure below, where the blue cones give the region where light travels from the source to the fiber. The mirrors are aligned so their axes of symmetry run vertically. However, because of the unique shape of the circular section, the cone of light that reaches the first mirror from the focal point is not symmetric around the horizontal. As seen in the diagram, the angle Theta 1 is larger than Theta 2. This becomes an issue in the design, because the source is housed in a cube, which has only a small aperture to allow light out. If the cube sits level, as it was designed, then the aperture is symmetric around the horizontal, and thus does not match the acceptance cone of the mirrors. This is easily remedied by tilting the source by about 4° as shown in

the bottom left of the figure. This misalignment, and the angle required to correct for it were discovered through the use of CAD models of the optical system.

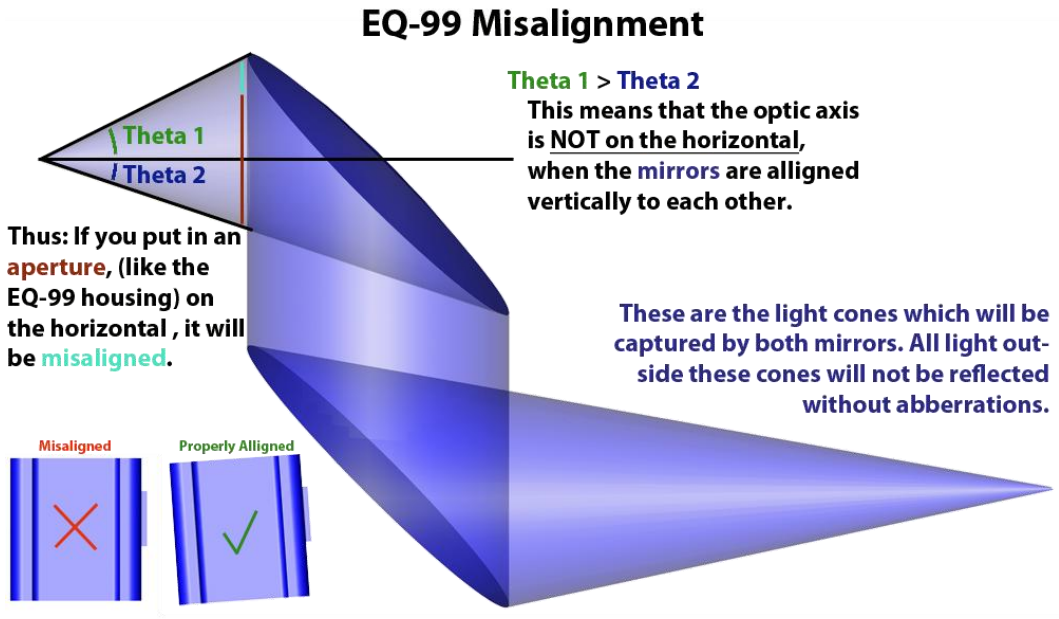

Figure A.1

APPENDIX B

MATLAB CODE FOR CALCULATING THE LIGHT DISTRIBUTION ON TEM SAMPLES

The process of designing a fiber tip cut and location which would effectively illuminate the sample was made much more efficient through the use of modeling to evaluate potential designs without the need to order multiple fibers, and test them experimentally. Modeling the light emitted from the tip of a fiber cut at an angle is not trivial. This is especially difficult because the diameter of the fiber tip is .6mm, while the distance to the sample is less than 3mm. This means that the tip cannot be considered a point source. It also should not be taken to be a lambertian source, since the radiant intensity is highly dependent on the angle the light is emitted at, and at large angles no light is emitted, as discussed in section 3.6 of the text.

To effectively model this complex light source, MATLAB was used to numerically work out this problem by dividing up the fiber tip into over 3000 pieces. Now, with each part of the fiber tip only about 1% as large it is more reasonable to take each of those parts to be point sources. The TEM sample is also divided up into over 3000 pieces, and the MATLAB code calculates the intensity reaching each point in the TEM sample from each point in the fiber. This is in principle quite easy to calculate, if it is assumed that every point in the fiber tip surface emits an equal amount of light, and that each point is a point source, and thus the intensity is inversely proportional to the distance from the point squared.

In the MATLAB code, 2 sets of points are produced, corresponding to the TEM sample and the fiber tip. The TEM sample is created by forming a grid of points, and then eliminating every point outside a certain radius from the origin. This circular grid is scaled appropriately, and then using matrix transformations, can be

tilted to any orientation, and moved to any location in space. The fiber tip is based on the same grid, but scaled to be smaller, and distorted and rotated to become the ellipse formed by an angled cut of a cylinder. The matrix used to rotate and shift the grid to the correct orientation and position is given in Eq B1, where ζ is the tilt angle around the sample rod axis, labeled y in the text (but z in the MATLAB code) and χ is the angle around the perpendicular x axis which is the direction the fiber comes into the microscope from (labeled x in both the text and the code) Δx, Δy, and Δz give the coordinates of the center of the grid.

$$\begin{matrix} \boldsymbol{\cos(\zeta)} & \boldsymbol{-\cos(\chi)\sin(\zeta)} & \boldsymbol{\sin(\chi)\sin(\zeta)} & \boldsymbol{\Delta x} \\ \boldsymbol{\sin(\zeta)} & \boldsymbol{\cos(\chi)\cos(\zeta)} & \boldsymbol{-\sin(\chi)\cos(\zeta)} & \boldsymbol{\Delta y} \\ \boldsymbol{0} & \boldsymbol{\sin(\chi)} & \boldsymbol{\cos(\chi)} & \boldsymbol{\Delta z} \\ \boldsymbol{0} & \boldsymbol{0} & \boldsymbol{0} & \boldsymbol{1} \end{matrix} \quad \text{(B1)}$$

Once these grids have been produced, and properly positioned in space relative to one another, the normal vectors to the surfaces are calculated and stored. Also calculated are the vectors and distances between each possible pair of TEM sample-fiber points. The angles between the 2 normal vectors and all the point-to-point vectors are then calculated.

As discussed in section 3.6 of the text, the maximum angles that light will exit the fiber tip are easily calculated from the index of refraction of the fiber core, and the acceptance angle of the fiber. Thus, it is simple to define a light direction vector at an angle with respect to the normal around which the limiting angles are symmetric. The angle between this direction vector and the point to point vectors can then be calculated, and for every vector for which this angle is larger than the maximum allowed, the intensity transmitted between those two points is

considered to be 0. For all the point pairs that fall within the angle limits, the intensity is inversely proportional to the distance between the pair of points. It is then important to correctly normalize the intensity values so that if the entire distribution lies within the TEM sample area, the sum of all the intensity values over the sample, multiplied by the area of the sample, is equal to the total power which is known to be emitted by the fiber. The equations that are used to calculate the intensity distribution are given here. In Eq B2 each additional term after the first is normalized to itself, so that the average of each term is equal to 1 and thus the summed value of P_{Sample} is unaffected. Eq B5 should be satisfied if the entire distribution falls on the sample area, and is the method used to check the normalizations.

$$\mathbf{I_{ij}} = \frac{\mathbf{P}}{\mathbf{N^2 * d_{ij}^2 (1-\cos(\phi_A)) 2\pi}} \frac{\mathbf{real}\left(\frac{\sqrt{\mathbf{1-n_c^2 \sin^2(\theta_{ij}^f)}}}{\mathbf{\cos(\theta_{ij}^f)}}\right)}{\mathbf{mean}\left(\mathbf{real}\left(\frac{\sqrt{\mathbf{1-n_c^2 \sin^2(\theta_{ij}^f)}}}{\mathbf{\cos(\theta_{ij}^f)}}\right)\right)} * \dots$$

$$\dots \frac{\mathbf{e^{-\left(\frac{r_i}{2\sigma}\right)^2}}}{\mathbf{mean}\left(\mathbf{e^{-\left(\frac{r_i}{2\sigma}\right)^2}}\right)} \frac{\mathbf{\cos(\theta_{ij}^T)}}{\mathbf{mean}\left(\mathbf{\cos(\theta_{ij}^T)}\right)} \quad \text{(B2)}$$

$$\mathbf{I_{ij}(\theta_{ij}^f > \phi_A) = 0} \quad \text{(B3)}$$

$$\mathbf{I_j = \sum_{i=1}^{N} I_{ij}} \quad \text{(B4)}$$

$$\mathbf{P_{Sample} = A_S * \sum_{j=1}^{N} I_j = P} \quad \text{(B5)}$$

In these equations, the following terms were used

I_{ij} –the intensity contributed to point j on the TEM sample by point i on the fiber tip

I_j –the total intensity at point j on the TEM sample

P –the power emitted from the fiber tip

P_{Sample} –the power reaching the TEM sample found by summing the intensities I_j

N –the number of points in the TEM sample grid and the fiber tip grid

d_{ij} –the distance from each point i in the fiber grid to each point j in the sample grid

r_i –the distance from the center of the fiber grid to the point i in the fiber grid

n_c –the index of refraction of the fiber core

σ –the standard deviation used for the Gaussian fiber tip emission

ϕ_A –the maximum angle from the fiber normal where light is still emitted

θ_{ij}^f–the angle between each light ray leaving the fiber and the fiber normal

θ_{ij}^T–the angle between each light ray striking the sample and the sample normal

The full code used is given below as is, and no line-by-line explanation will be given, besides that which has already been written into the code to aid my own recollection and make it easier to edit.

```
%Dimensions are in microns
clear
%XXXXXXXXXXXXXXXXXXXXXXXXXXXXXXXXXXXXXXXXXXXXXXXXXXXXXXXXXXXXXXXXXXXXXXX
%Parameters
%Get Spectra From File... ask User for Columns
%Default is EQ-99, 2m fiber optic, and 2 parabolic mirrors, no
filter
%!!Careful... computation time scales as MeshSpacing^-4
%Do not go much lower than 50
FiberNA=.187;
NAA=asin(FiberNA);
MeshSpacing=50;
DiamT=3000;
DiamF=600;
AcceptAngle=NAA*180/pi;
```

```
TEMScale=.835/1.5;
TEMScale=2
FScale=1;
Col=input('What are the collumn numbers of the desired spectra in
the Spectrum Data File? (Row Vector)');
if isempty(Col)
    Col=[2,6,7,7];
end
%Call function to get power from spectra
[P,nCore]=PowerIntegrate(Col);
%Reduce Power because of coupling inefficiency
P=.1815*P*.5;
for i=1:1
PosShift=(i-1)*[0 -250 0];

chiF=0*pi/180;
gammaF=0;
%zetaf is angle between fiber direction and horizontal
zetaf=-15;
zetaF=-(pi/2-zetaf/180*pi);
%Position Based on Measured beam angle
PosF=1000*[2.553,-1.923,0];
PosF=PosF+PosShift;
PositionFiber(i,:)=PosF;
zetaT=0;
%positive chiT dips the far edge of the sample down
chiT=0/180*pi;
gammaT=0/180*pi;
zetaT=-(zetaT/180*pi);
%TEM Translation
TEMTRANS=[0,0,0];
if isempty(TEMTRANS)
    TEMTRANS=[0,0,0];
end
dxT=TEMTRANS(1,1); dyT=TEMTRANS(1,2); dzT=TEMTRANS(1,3);

CutQ=1;
%XXXXXXXXXXXXXXXXXXXXXXXXXXXXXXXXXXXXXXXXXXXXXXXXXXXXXXXXXXXXXXXXXXXXXXX
%XXXXXXXXXXXXXXXXXXXXXXXXXXXXXXXXXXXXXXXXXXXXXXXXXXXXXXXXXXXXXXXXXXXXXXXX
%Rotation Matrices
RzF=[cos(zetaF) -sin(zetaF) 0
sin(zetaF) cos(zetaF) 0
0 0 1];
RxF=[1 0 0
0 cos(chiF) -sin(chiF)
0 sin(chiF) cos(chiF)];
RyF=[0 0 0
    0 0 0
    0 0 0];
Rx=[1 0 0
0 cos(chiT) -sin(chiT)
0 sin(chiT) cos(chiT)];
Ry=[cos(gammaT) 0 sin(gammaT)
0 1 0
-sin(gammaT) 0 cos(gammaT)];
Rz=[cos(zetaT) -sin(zetaT) 0
```

```
sin(zetaT) cos(zetaT) 0
0 0 1];
%XXXXXXXXXXXXXXXXXXXXXXXXXXXXXXXXXXXXXXXXXXXXXXXXXXXXXXXXXXXXXXXXXXXXXXX
%XXXXXXXXXXXXXXXXXXXXXXXXXXXXXXXXXXXXXXXXXXXXXXXXXXXXXXXXXXXXXXXXXXXXXXXX
%Translation Vector
Txyz=[dxT;dyT;dzT];
%Rx performed first
TM=Rz*Rx;
%Transformation Matrix
TM=[TM,Txyz;0 0 0 1];

%Initial Meshing
bbox=[-.5*DiamT,-.5*DiamT;.5*DiamT,.5*DiamT];
[x,y]=meshgrid(bbox(1,1):MeshSpacing:bbox(2,1),bbox(1,2):MeshSpac
ing*sqrt(3)/2:bbox(2,2));
x(2:2:end,:)=x(2:2:end,:)+MeshSpacing/2;
p=[x(:),y(:)];
x=p(:,1);
y=p(:,2);
%Eliminate Outside of Circle
Distance=(x.^2+y.^2).^(.5);
X=x(Distance<DiamT/2);
Z=y(Distance<DiamT/2);
%Calculate Distance Squared for gaussian dist
DistanceSq=(X.^2+Z.^2);

%Check if there are too many points... because of memory
constraints
if length(X)>4000
    error('Too many Points... Change the MeshSpacing to a higher
value')
end
%Create TEM,Fiber Gridding
Y=ones(length(X),1);
Fibergridflat=DiamF/DiamT*[X';(Y-Y)';Z'];
TEMgridflat=[X';(Y-Y)';Z'];
TEMgridflat=[TEMgridflat;Y'];
%Scale grid to use smaller portion on sample area, and eliminate
4th row of matrix
TEMgrid=TM*TEMgridflat;
if ~exist('TEMScale','var')
TEMgrid=TEMgrid(1:3,:);
else
TEMgrid=TEMScale*TEMgrid(1:3,:);
end

%Position and Rotation of Grids
if isempty(CutQ)
else
   if CutQ==1
   CutA=30;
   CutA=CutA*pi/180;
   Theta1=(asin(nCore*sin(CutA+asin(sin(NAA)/nCore)))-
CutA)*180/pi;
   Theta2=(asin(nCore*sin(CutA-asin(sin(NAA)/nCore)))-
CutA)*180/pi;
```

```
    AcceptAngle=.5*abs(Theta1-Theta2);
    CNA=-44.1/180*pi;
    ScaleCut=1/cos(CutA);
    Fibergridflat=diag([ScaleCut,1,1])*Fibergridflat;
    Fibergridflat=diag([FScale,FScale,FScale])*Fibergridflat;
    RzFC=[cos(CutA) -sin(CutA) 0
    sin(CutA) cos(CutA) 0
    0 0 1];
    RN=[cos(CNA) -sin(CNA) 0
        sin(CNA) cos(CNA) 0
        0 0 1];
    Fibergridflat=RzFC*Fibergridflat;
    else
        error('CutQ must be either 1 or left blank')
    end
end
Fibergrid=RzF*Fibergridflat;
%Translate Fiber end to Specified Position
SF=size(Fibergrid,2);
TransF=[PosF(1)*ones(SF,1),PosF(2)*ones(SF,1),PosF(3)*ones(SF,1)]
';
Fibergrid=Fibergrid+TransF;
Fibergrid=RxF*Fibergrid;

%Vectors for Plotting
XT=TEMgrid(1,:);
YT=TEMgrid(2,:);
ZT=TEMgrid(3,:);
XF=[Fibergrid(1,:),0];
YF=[Fibergrid(2,:),0];
ZF=[Fibergrid(3,:),0];
XA=[XT,XF];
YA=[YT,YF];
ZA=[ZT,ZF];

%Produce Vectors for Angle Calculation
A=[XF(1,1)-XF(1,2);YF(1,1)-YF(1,2);ZF(1,1)-ZF(1,2)];
B=[XF(1,7)-XF(1,71);YF(1,7)-YF(1,71);ZF(1,7)-ZF(1,71)];

FNorm=cross(B,A);
if ~exist('CutQ','var');
else
    if CutQ==1
        FNorm=RN*FNorm;
        FNorm=-FNorm;
    end
end

A=[XT(1,1)-XT(1,2);YT(1,1)-YT(1,2);ZT(1,1)-ZT(1,2)];
B=[XT(1,7)-XT(1,71);YT(1,7)-YT(1,71);ZT(1,7)-ZT(1,71)];
TNorm=cross(A,B);
TNorm=-TNorm;
NormsCosine=sum(FNorm.*TNorm)/norm(FNorm)/norm(TNorm);
NormsAngle=180/pi*acos(NormsCosine);
TEMCenterD=(TEMgrid(1,:).^2+TEMgrid(2,:).^2+TEMgrid(3,:).^2).^(1/
2);
```

```
[TDmin,TC]=min(TEMCenterD);

%Calculation of Intensities
%Calculate Distance Between Points
d21=ones(length(Fibergrid),1)*Fibergrid(1,:).^2-
TEMgrid(1,:)'*2*Fibergrid(1,:)+TEMgrid(1,:)'.^2*ones(1,length(Fib
ergrid));
d22=ones(length(Fibergrid),1)*Fibergrid(2,:).^2-
TEMgrid(2,:)'*2*Fibergrid(2,:)+TEMgrid(2,:)'.^2*ones(1,length(Fib
ergrid));
d23=ones(length(Fibergrid),1)*Fibergrid(3,:).^2-
TEMgrid(3,:)'*2*Fibergrid(3,:)+TEMgrid(3,:)'.^2*ones(1,length(Fib
ergrid));
d=(sqrt(d21+d22+d23))';

%Calculate Vectors Between Points
Vect1=Fibergrid(1,:)'*ones(1,length(Fibergrid))-
ones(length(TEMgrid),1)*TEMgrid(1,:);
Vect2=Fibergrid(2,:)'*ones(1,length(Fibergrid))-
ones(length(TEMgrid),1)*TEMgrid(2,:);
Vect3=Fibergrid(3,:)'*ones(1,length(Fibergrid))-
ones(length(TEMgrid),1)*TEMgrid(3,:);
Vect=cat(3,Vect1,Vect2,Vect3);
%Calculate Angle Between Vectors and Fiber-End Normal
VAngle=acos((FNorm(1)*Vect1+FNorm(2)*Vect2+FNorm(3)*Vect3)./(norm
(FNorm)*(Vect1.^2+Vect2.^2+Vect3.^2).^(.5)));

%Calculate Angle Between Vectors and TEM Sample Normal
VAngleT=acos((TNorm(1)*Vect1+TNorm(2)*Vect2+TNorm(3)*Vect3)./(nor
m(TNorm)*(Vect1.^2+Vect2.^2+Vect3.^2).^(.5)));
%Set x Component of Vectors between points to 0... to calculate
Second Fiber angle
Vect(:,:,2)=0;
VAngleFlat=acos(Vect1./((Vect1.^2+Vect3.^2).^(.5)));

%Power per emmitter element
p=P/length(X);
pF=p/(2*pi*(1-cos(AcceptAngle*pi/180)))*4*pi;
%Gaussian Distribution of fiber end intensity
Sigma=max(DistanceSq);
Gauss=exp(-.5*DistanceSq/Sigma/2);
Gauss=Gauss/mean(Gauss);
GaussM=Gauss*ones(1,length(Gauss));
%Other Angular Factors Influencing Intensity
VAngleDist=real(sqrt(1-nCore^2*(sin(VAngle)).^2)./cos(VAngle));
VAngleDist=VAngleDist/mean(mean(VAngleDist));
CosFactor=abs(cos(VAngleT))/mean(mean(cos(VAngleT)));
%Intensity (mW/cm^2)
I=pF/4/pi./d.^2*10^8.*CosFactor.*GaussM.*VAngleDist;
I(abs(VAngle)>AcceptAngle*pi/180)=0;
ITEM=(sum(I,1));
IAv=sum(ITEM)/length(ITEM);
if ~exist('TEMScale','var')
    Itot=IAv*.15^2*pi;
elsede
    Itot=IAv*(.15*TEMScale)^2*pi;
```

```
end
ITotal=num2str(Itot);
ICenter=ITEM(TC);

[IM,Imax]=max(ITEM);
ImaxCoord(:,i)=TEMgrid(:,Imax);

%XXXXXXXXXXXXXXXXXXXXXXXXXXXXXXXXXXXXXXXXXXXXXXXXXXXXXXXXXXXXXXXX
%XXXXXXXXXXXXXXXXXXXXXXXXXXXXXXXXXXXXXXXXXXXXXXXXXXXXXXXXXXXXXXXX
%Plotting

figure (3)
scatter3(XT,YT,ZT,[],ITEM,'filled')
set(gca,'cameraupvector',[0,-1,0])
axis equal
h=colorbar('location','westoutside');
set(gca,'XDir','rev','YDir','rev','ZDir','rev')
title('TEM Sample Irradiance (mW/cm^2)')
set(3,'name','TEM Sample Irradiance')
In=num2str(PositionFiber(i,2));
SaveAs=strcat('FiberDist',In,'.bmp');
%save the figure as a bitmap file
print(SaveAs, '-dbmp')
end

figure (4)
IAll=[ITEM,min(ITEM)*ones(1,length(XF))];
scatter3(XA,YA,ZA,[],IAll)
set(gca,'cameraupvector',[0,-1,0])
axis equal
colorbar('westoutside')
set(gca,'XDir','rev','YDir','rev','ZDir','rev')
title(strcat('TEM Sample Irradiance (mW/cm^2)   Total Power
(mW)=',ITotal))
set(4,'name','Spatial Representation Sample Irradiance')

figure (5)
scatter3(XT,ZT,ITEM,200,ITEM,'filled')
axis square
xlabel('Fiber Direction')
ylabel('Sample Rod Direction')
zlabel('Irradiance (mW/cm^2)')
title('TEM Sample Irradiance')
set(5,'name','Intensity Distribution Surface')

figure (6)
scatter3(XT,ZT,Gauss,200,Gauss,'filled')
axis square
xlabel('X')
ylabel('Z')
zlabel('Relative Irradiance (a.u.)')
title('Fiber End Irradiance')
set(6,'name','Fiber End Intensity Distribution Surface')
```

APPENDIX C

INTENSITY CONVERSION FACTOR MATLAB CODE

The following MATLAB code takes input from the user about the various optical components, including filters that are to be considered. This is input by specifying the column numbers from a text file, which has been produced using Excel, and has the spectral data from all the optical components used in the system in columns. The code outputs a plot showing the spectrum resulting from the chosen optical components, as well as several variables. The total power, 'PowerSpecLim', the conversion factor for the Thorlabs photodetector, 'LinF', and the conversion factor for the photodiode, 'LinFSH', are output to the MATLAB workspace.

```
function
[PowerSpecLim,LinF,LinFSH]=PowerIntegrate(Col)
DataID=fopen('MATLAB_Data.txt');
Data=textscan(DataID,'%f %f %f %f %f %f %f %f %f %f %f
%f %f %f %f %f %f %f %f %f %f %f %f %f %f %f %f %f %f
%f','headerlines',1);
Spectra=[Data{1},Data{2},Data{3},Data{4},Data{5},Data{
6},Data{7},Data{8},Data{9},Data{10},Data{11},Data{12},
Data{13},Data{14},Data{15},Data{16},Data{17},Data{18},
Data{19},Data{20},Data{21},Data{22},Data{23},Data{24},
Data{25},Data{26},Data{27},Data{28},Data{29},Data{30}]
;
CompSpec=ones(size(Spectra,1),1);
for i=1:length(Col)
CompSpec=Spectra(:,Col(i)).*CompSpec;
end

PowerSpecLim=sum(CompSpec)/2
PString=num2str(PowerSpecLim,4);

figure (2)
semilogy(Spectra(:,1),CompSpec,'linewidth',5)
title(strcat('Composite Spectrum   Total Power
(mW)=',PString))
xlabel('Wavelength (nm)')
ylabel('Spectral Power (mW/nm)')
set(1,'name','Composite Spectrum')
```

```
NormSpec=CompSpec/sum(CompSpec);
Ohm=50000;
DetArea=.05^2*pi;
DetArea2=.0516;
LinF=1/Ohm/DetArea/sum(NormSpec.*Spectra(:,23));
%Use .001 because measured in uA rather than mA
LinFSH=.001/DetArea2/sum(NormSpec.*Spectra(:,27));
```

APPENDIX D

IN-SITU LIGHT MEASUREMENT PHOTODIODE HOLDER

Inside the TEM column it is difficult to determine whether or not the light beam is actually positioned correctly on the TEM sample. We are capable of precisely positioning the fiber tip using the manipulator described in section 3.5 of the text, but characterizing where the light maximum is on the sample plane requires another piece of equipment. The procedure for aligning the fiber using a photodiode housed in a sample holder was given in section 4.4 of the text, but the details of this holder, and of the photodiode will only be given here.

The photodiode used to measure intensities in situ was produced by Hammamatsu and is the S1087-01. This diode has a spectral response range from about 320nm to 1100nm. The active area is about 1.6mm^2, and the entire ceramic casing is about 5x6mm. The holder used to house this diode was an old, and no longer used, liquid nitrogen holder. The holder came already equipped with wires which ran along the sample rod, into the body of the holder. There they were attached to contacts which are accessible from the outside of the holder. These wires along the rod were spliced with new wires, which reach to the sample area and are soldered on to the diode leads. Another set of wires, visible in the photo below are connected to the external contacts, and when in use, are connected to a multimeter to measure the current from the diode.

Before the photodiode could be added to the holder, all the original mechanism for securing and tilting the sample had to be removed. The ceramic casing of the photodiode was slightly too large for the sample holder, so it was ground down to fit snugly in the holder. Finally, the holes through which the wires pass into the sample rod were sealed with Torr Seal, a vacuum epoxy, which ensures that the

holder does not leak air into the TEM column, because the original seals in the holder seem to have failed.

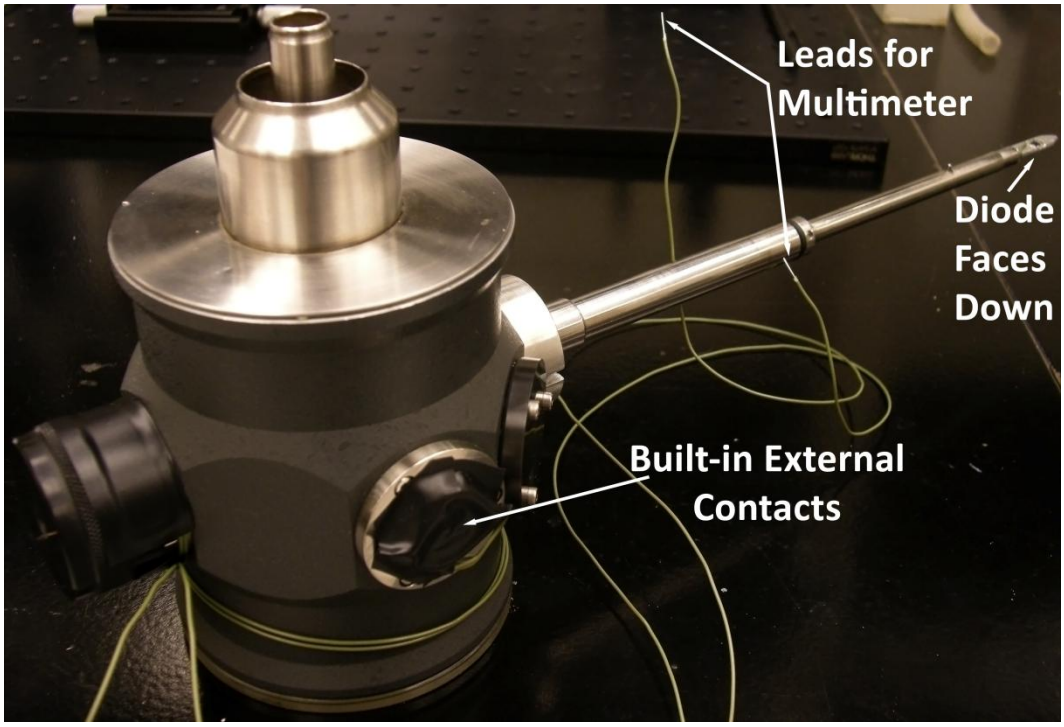

Figure D.1